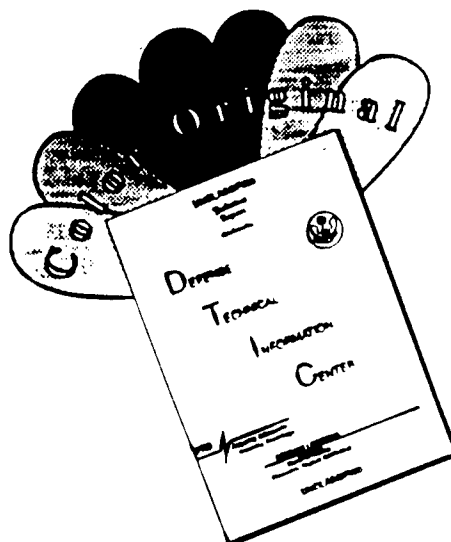




# DISCLAIMER NOTICE



THIS DOCUMENT IS BEST QUALITY AVAILABLE. THE COPY FURNISHED TO DTIC CONTAINED A SIGNIFICANT NUMBER OF COLOR PAGES WHICH DO NOT REPRODUCE LEGIBLY ON BLACK AND WHITE MICROFICHE.

## ABSTRACT

KROGH, TONY CHRISTIAN. Determination of Frontal Structure in the Mid-Atlantic Region from WSR-88D Doppler Radar Velocity Azimuth Displays. (Under the direction of Steven E. Koch.)

This research develops a technique for using the WSR-88D Doppler Radar to study cold air damming events in the mid-Atlantic region. Of particular use is the Velocity-Azimuth Display Wind Profile (VWP), which is a time-height plot of horizontal winds above the radar at ~300 m intervals. VWPs were gathered from seven stations across the region for this study.

A thermal retrieval technique is employed using the vertical wind shears obtained from VWPs, along with the thermal wind equation, to retrieve the horizontal thermal gradients  $\nabla_r T$  and the associated horizontal thermal advections. VWP winds are height referenced, so the rawinsonde stations are used for conversion to pressure coordinates. Multiple height map analyses of thermal fields are constructed as well as single station time-height analyses of temperature gradients, thermal advections, and isentropes. Several methods were explored for the recovery of the horizontal temperature field from the  $\nabla_r T$ -wind relationship.

The retrieval technique is applied to two cold air damming events: December 18-19, 1995 and January 6-7, 1996. Both of these events were major winter storms for the east coast of the United States. The resulting thermal fields are verified by comparing them with surface analyses, NWS upper air analyses, and mesoscale model initial analyses and forecast fields. The comparisons of the retrieved thermal fields with currently available products was good, and shows the technique to be of use. Retrieved

temperature advections at 850 mb matched well with NWS 850 mb analyses. The retrieved temperatures proved to be less reliable than the temperature advections because of the additional assumptions required to reconstruct the temperature field. Nevertheless, time-height cross sections of the reconstructed isentropes at the radar sites were found to be consistent with stability changes implied by the thermal advection cross sections. Furthermore, excellent time-height continuity was displayed in most of the time cross sections. The greatest value of the retrieval technique lies in the fact that the retrieved thermal fields are available hourly, as opposed to the operational rawinsonde network which provide data only every 12 hours.

This retrieval method is limited by making the geostrophic assumption for the wind field. Errors become large in areas of strong curvature and ageostrophy. Error analysis of curvature showed curvature to be negligible in these cases. Also, although it is highly desirable to use VWP winds from the lowest levels because the cold air associated with these winter systems is shallow, ageostrophy due to friction can't be ignored. Error analysis of friction, at one station, showed friction only to be negligible above ~600 m. Finally, round-off error is introduced because of the necessary reliance upon VWP analog displays of wind vectors.

**DETERMINATION OF FRONTAL STRUCTURE IN THE MID-  
ATLANTIC REGION FROM WSR-88D DOPPLER RADAR  
VELOCITY AZIMUTH DISPLAYS**

by

**TONY CHRISTIAN KROGH**

A thesis submitted to the Graduate Faculty of  
North Carolina State University  
in partial fulfillment of the  
requirements for the Degree of  
Master of Science

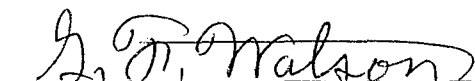
**MARINE, EARTH AND ATMOSPHERIC SCIENCES**

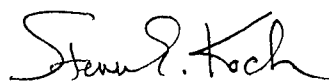
Raleigh

1996

**APPROVED BY:**

  
Alan J. Riordan

  
Gerald F. Watson

  
Steven E. Koch  
Chairman of Advisory Committee

## **Dedication**

I would like to dedicate, first and foremost, this thesis to the Lord Jesus Christ, without whom I could do nothing. This last two years I have carried long hours and large amounts of stress, which has left me with little time for my family. My precious wife has graciously handled the task of keeping our home and caring for our children, as well as, giving birth to our third child during my last semester of classes. Therefore, this thesis is also dedicated to my loving wife, Alycia, my two boys, Joshua and Caleb, and my precious new daughter, Kymberly. Your love, support and prayers have pushed me and helped me to attain this goal. Thank you.

---

### **Biography**

Tony Christian Krogh is an Officer in the United States Air Force assigned to the Air Force Institute of Technology and works as a Weather Officer.

He [REDACTED] and lived in many locations as his family moved around during his childhood. Tony enlisted in the United States Air Force (USAF) on 23 February 1983. In 1988, he was selected by the Air Force Institute of Technology to attend the University of Arizona and received a Bachelors Degree in Atmospheric Science. After graduation in 1991, he attended the AF Officers Training School and was commissioned as a Second Lieutenant in the AF in June 1991. He was then assigned to work at the Headquarters for the U. S. Strategic Command located at Offutt AFB, NE and worked as a Meteorological and Oceanographic Readiness Officer. Tony was promoted to the rank of Captain in June 1995. While at Offutt AFB, he was selected by AFTT to attend North Carolina State University to obtain an advanced degree in Meteorology.

Upon completion of his Masters Degree, Tony will be assigned to the National Air Intelligence Center located at Wright-Patterson AFB, OH, where he will use his weather knowledge in the intelligence field.

Tony C. Krogh is married to the former Alycia Gaye Devers of Louisville, KY. They have three children, Joshua [REDACTED], Caleb [REDACTED], and Kymberly [REDACTED].

## Acknowledgments

A thesis of North Carolina State University pursuant to University Corporation for Atmospheric Research (UCAR) Subaward No. S96-75675 pursuant to National Oceanic and Atmospheric Administration Award No. NA57GP0567.

This paper is funded in part from a subaward under a cooperative agreement between the National Oceanic and Atmospheric Administration and the University Corporation for Atmospheric Research (UCAR). The views expressed herein are those of the author and do not necessarily reflect the views of NOAA, its sub-agencies, or UCAR.

I would first like to thank the United States Air Force and Air Force Institute of Technology for allowing me the opportunity to obtain this degree. Without their support this goal would have been a long time in coming.

I would also like to express my appreciation to my advisory committee, Dr. Steven E. Koch (Chairman), Dr. Allen J. Riordan, and Dr. Gerald F. Watson. Their guidance and personal interest in this work were instrumental in the successful completion of this research.

I would like to acknowledge the men and women of the NWS Raleigh office. They never hesitated to answer questions or go out of their way to help find an answer. The professionalism and dedication they displayed were commendable. The following individuals directly contributed to this research by providing operational input, assistance on data collection and/or providing key information: Ed Delgado, Rod Gonski, Ron Humble, Jim Merrel, and Jan Price.

I would also like to acknowledge Gail Hartfield and Kermit Keeter who acted as my NWS liaison for this work. Their knowledge of cold air damming provided key insight for this study. Their willingness to help at whatever time I needed it was greatly appreciated. Thanks Gail and Kermit.



I would like to thank Steve Harned and again thank Kermit Keeter, the Meteorologist in Charge and the Science and Operations Officer (SOO) respectively, of the NWS Raleigh Office. Because of their desire to support this research and the collaborative efforts between the National Weather Service and North Carolina State University, they opened their office to me and provided support throughout the study. They ultimately made this study both possible and successful.

Lastly, many things would not have gotten accomplished without assistance from my fellow students. I would like to thank: Mike Adams, Devin Kramer, Bob Rozumalski, Leanne Siedlarz, Mike Trexler, and Chris Vandersip. Your expertise and encouragement were helpful in so many areas, and I am grateful to you all.

## TABLE OF CONTENTS

	<u>Page</u>
LIST OF FIGURES .....	vii
1. INTRODUCTION .....	1
2. LITERATURE REVIEW .....	3
2.1 Cold Air Damming .....	3
2.2 Carolina Coastal Front .....	6
2.3 Retrieving Horizontal Temperature Gradients from Profilers .....	7
2.4 Velocity Azimuth Display (VAD) Wind Profiles (VWP) .....	8
3. DATA .....	11
3.1 Rawinsonde Data .....	11
3.2 VWP Data .....	12
3.3 Mesoscale Model Data .....	13
4. ANALYSIS TECHNIQUES .....	15
4.1 Temperature Gradient and Temperature Advection Retrievals .....	15
4.2 Temperature and Potential Temperature Field Reconstruction .....	17
5. CASE STUDIES .....	20
5.1 December 18-19, 1995 .....	20
5.2 January 6-7, 1996 .....	24
6. CONCLUSIONS .....	30
7. REFERENCES .....	61

## List of Figures

	<u>Page</u>
Figure 2.1 Topography of southeastern United States .....	32
Figure 2.2 Example of CAD as seen on a surface analysis .....	33
Figure 2.3 Depiction of CAD flow pattern .....	34
Figure 2.4 Example of Carolina Coastal front position and temperature gradient .....	35
Figure 2.5 Geometry of VAD .....	36
Figure 2.6 VAD Wind Profile .....	37
Figure 3.1 Locations of radar sites and rawinsonde sites .....	38
Figure 3.2 Wind averaging error analysis graph .....	39
Figure 4.1 Order of radar site temperature calculations .....	40
Figure 5.1 Surface analysis for 19 December 1995 at 0600 and 0900 UTC .....	41
Figure 5.2 Surface analysis for 1200 and 1500 UTC .....	42
Figure 5.3 Surface analysis for 1800 UTC .....	43
Figure 5.4 Retrieved isotherm analysis at 850 mb for 1200 and 1800 UTC .....	44
Figure 5.5 850 mb upper air analysis and MASS 850 mb analysis for 1200 UTC ...	45
Figure 5.6 Retrieved temperature advection cross sections .....	46
Figure 5.7 Retrieved temperature advection cross sections .....	47
Figure 5.8 Retrieved isentropic cross sections .....	48
Figure 5.9 Retrieved isentropic cross sections .....	49
Figure 5.10 Balance of surface forces in CAD .....	50
Figure 5.11 Potential temperature plots .....	51
Figure 5.12 Surface analysis for 6 January 1996 at 2100 and 7 January at 0000 UTC .....	52
Figure 5.13 Surface analysis for 0300 and 0600 UTC .....	53
Figure 5.14 Surface analysis for 0900 and 1200 UTC .....	54
Figure 5.15 Radar composite for 0000 and 0900 UTC.....	55

Figure 5.16 Retrieved isotherm analysis and upper air analysis at 850 mb for 0000 UTC .....	56
Figure 5.17 Retrieved temperature advection cross sections .....	57
Figure 5.18 Retrieved temperature advection cross sections .....	58
Figure 5.19 Retrieved isentropic cross sections .....	59
Figure 5.20 Retrieved isentropic cross sections .....	60

## 1. INTRODUCTION

Winter weather systems in the Carolinas can be complicated. Because of the Appalachian Mountains to the west, and the Atlantic Ocean and Gulf Stream to the east, many unique weather situations occur. One especially important event is cold air damming along the lee of the mountains, often accompanied by a coastal front pushing in from the Atlantic. This situation presents many forecasting problems. The greatest obstacle to improving forecasting for these situations has been inadequate space and time resolution of upper air data. This has led to an inadequate understanding of the three-dimensional structure and dynamics of these features.

One of the major forecast challenges is the onset and evolution of cold air damming (CAD) (Forbes et al. 1987; Bell and Bosart 1988). CAD typically occurs when a synoptic high pressure system moves into the northeastern US, bringing cold air southward into the Mid-Atlantic region which becomes entrenched along the eastern slopes of the Appalachians. The location and persistence of this cold air can cause many problems in forecasting temperatures and precipitation types. Some of the main tools for forecasting CAD are products prepared using the National Weather Service's (NWS) rawinsonde network. The results of using the synoptically-spaced (~400 km) 12-hr soundings to predict this phenomenon have been poor, as have the attempts to use operational forecast models (Keeter et al. 1995).

With the installation of the WSR-88D Doppler Radar network across the Mid-Atlantic region, a large amount of new information has become available to study these winter weather systems. The purpose of the present study is to exploit some of the information available from the WSR-88D, specifically the Velocity-Azimuth Display (VAD) Wind Profile (VWP). This product is an average wind over an area covered by the radar in horizontal slices at different levels. It gives winds at 1,000 ft. (305 m) intervals every 5-10 minutes.

The VWP thermal retrieval technique used in this research can provide baroclinic information on an hourly basis, rather than 12 hr as available from the operational rawinsonde network, and with somewhat better spatial resolution (spacing ~240 km). The objectives of the present research are to (1) use the Neiman and Shapiro (1989) thermal gradient retrieval technique to retrieve horizontal temperature gradients from VWP's during two wintertime CAD events in the mid-Atlantic region; (2) develop a temperature recovery technique to obtain the temperature field from the temperature gradients in the two case studies; (3) prepare time-height cross section and map analysis products for temperature, temperature advection, and potential temperature; and (4) compare results to standard operationally available products (12-hourly rawinsonde analyses, mesoscale model initial and forecast fields, and 3-hourly surface analyses) for physical consistency and agreement with observed surface conditions.

A brief history of CAD and the Carolina coastal front, earlier attempts to employ the thermal retrieval technique using wind profiler data, and the VWP technique are discussed in section 2. The data used in this study are described in section 3. Specifics concerning the thermal retrieval techniques used to retrieve temperature gradients, temperature advections, temperatures, and potential temperatures and discussion of potential sources of error appear in section 4. Results from applying the technique to two case studies appear in section 5, followed by the concluding remarks.

## 2. LITERATURE REVIEW

### 2.1 Cold Air Damming

The phenomenon of cold air becoming entrenched along the slopes of mountain ranges is referred to as cold-air damming (Richwien 1980). The topography of the southeastern United States can be roughly characterized by geographical zones as illustrated in Fig. 2.1 (from Dirks et al. 1988). The Appalachian Mountains are the main orographic boundary in the western area of concern with typical heights of 1.0 km to 1.5 km and a maximum height of ~2 km at Mt. Mitchell, NC. The Appalachian, Piedmont, and Coastal Plain zones are all aligned almost parallel to the coast and they are each 100 km to 150 km wide. The Gulf Stream, which is also approximately parallel to the coast, is about 100 km wide and occurs over the "break" in the continental shelf.

The interaction of the Gulf Stream with the overlying atmosphere is complex and not fully understood. The Gulf Stream parallels the coast for about 1200 km, from Key West, FL to Cape Hatteras, NC (Knauss 1978). The Gulf Stream surface temperatures remain at 20-25°C year round with strong horizontal thermal gradients (up to 1°C per km) observed between the Gulf Stream and the continental shelf during the winter. The western edge of the stream is easily identifiable because of this horizontal temperature gradient, thus the term "Gulf Stream front". As the Gulf Stream meanders and frontal eddies move through the stream, mesoscale variability in sea surface temperature and evaporation rates occur (Dirks et al. 1988). This variability is evident since the Gulf Stream's sea surface temperature front can be displaced as much as 40 km from the mean position of the stream (Bane and Brooks 1979). A small shift in the strength or position of the Gulf Stream will affect the overall ocean-atmosphere heat balance (Bauman 1989).

A ridge of high pressure, which can be identified by U-shaped isobars on a surface analysis, characterizes damming events that occur along the eastern slopes of the Appalachian Mountains (Fig. 2.2). The temperature difference between the damming

region and the coast (~150 km) can exceed 20°C. As a result, the depth and structure of the cold dome can be a critical factor in distinguishing a rain event from a sleet or freezing rain event as liquid precipitation passes through the cold dome and freezes or becomes supercooled (Penn 1957; Chainé 1973; Forbes et al. 1987; Fritsch et al. 1992).

Bell and Bosart (1988) used a 50-year climatology to show that in the Virginia-Carolinas region of the eastern slopes of the Appalachian Mountains damming can occur in any month of the year. Over two-thirds of all damming events and damming days occurred between October and April. The winter months, especially March and December, are five times more likely, on the average, to experience a strong event than July. The summer damming episodes are neither as intense nor as prolonged as their winter counterparts.

Keeter et al. (1995) explained damming this way. An upper-level split flow pattern, consisting of two distinct and separate jet streams, often exists across North America during damming episodes. The confluence of the two streams along the east coast produces mass convergence aloft that enhances the polar anticyclone as it tracks eastward toward the coast. The damming develops when cold air flowing southward on the east side of the anticyclone encounters the mountains. As the cold air builds up against the mountains, the air is forced to move southward east of the barrier, creating a "wedge" of high pressure (sometimes referred to as a Baker ridge). This southward movement of the air is highly ageostrophic and more or less in the direction of the pressure gradient force. This flow results from the deceleration of the wind due to increased friction as the air approaches the mountain slopes (Bell and Bosart 1988). This force imbalance between Coriolis and pressure gradient causes the wind to accelerate southwestward, in the direction of the stronger pressure gradient force. Adiabatic cooling, due to this upslope component of the boundary-layer flow, and evaporative cooling of precipitation falling below the clouds, together help to maintain the cold dome. Since the inversion at the top of the cold air slopes downward to the east, a barrier jet, which is a low-level wind maximum parallel



to the terrain contours (i.e., northeast wind), may develop near the base of the inversion. This jet forms in response to the geostrophic winds on the east side of the damming pressure ridge in combination with the orographic channeling. The sloping inversion often appears to be an elevated extension of the coastal front (Forbes et al. 1987). There was no evidence of any such barrier jet in the WSR-88D data analyzed in this study, though no attempt was made to understand why this was the case.

Figure 2.3 shows the typical low-level flow patterns associated with cold-air damming events. Warm moist air flowing northeastward from the Gulf of Mexico, or westward from over the Gulf Stream, overruns the cold air dammed against the eastern slopes of the Appalachians. This frontal ascent typically results in extensive and persistent low cloudiness and stratiform precipitation. The surface flow for CAD is normally highly ageostrophic, especially during the onset of the event. During strong damming events, the shallow boundary along the eastern and southern periphery of the cold air dome is typically found in the coastal area of the Carolinas. For weaker events, or even as a strong cold dome erodes, the shallow boundary is often located inland over the Piedmont or coastal plain regions. Strength of CAD events is not so much correlated with its depth as it is with the resistance of the cold dome to erosion.

A spectrum of cold air damming events has been suggested recently by Hartfield et al. (1995). "Classical" cold air damming events are initiated and maintained by synoptic-scale features that include: i) a connecting/supporting surface parent high over New England; ii) confluent flow at 500 mb above the parent high and; iii) superpositioning of the thermally direct and indirect circulations associated with the entrance region of the polar jet and the exit region of the subtropical jet. "In situ" damming events are categorized as those CAD events that are initiated with little or no support from the prevailing synoptic-scale features. As a result, there is no significant advection of cold, stable air into the damming region. The indirect effects of diabatic evaporational cooling on the air mass already in place is

thought to lead to “in situ” damming, augmented by cooling caused by upslope flow in some cases. “Hybrid” damming events are due to the combined contributions from both diabatic cooling processes and weak horizontal cold air advection (into the damming region) provided by the rather limited support from somewhat favorable synoptic features. When the synoptic support is weak, often it is evaporative cooling from precipitation that tips the scales toward the development of a damming event (Fritsch et al. 1992).

Damming look-alikes include cool air pooling produced by diabatic processes acting alone or in combination with upslope cloudiness produced solely by orographic ascent. The presence of cloudiness (and precipitation) within the cool air region, in contrast to less cloudy conditions in the warm sector, helps to maintain the thermal contrast across the front and may help to initiate strong frontal convection (Businger et al. 1991; Koch et al. 1996)

## **2.2 Carolina Coastal Front**

Riordan (1996) describes the coastal front as a shallow, but intense, baroclinic zone that forms along the east coast of the United States in winter. The coastal front marks the transition between a warm, statically less stable maritime air mass and a cold, more stable continental air mass that lies to the west. Temperature contrasts across the front attain as much as 10°C over a short distance of 50 km.

Offshore of the Carolinas, frontogenesis is frequently observed in the vicinity of the Gulf Stream (e.g., Bosart et al. 1972; Bosart 1975; Marks and Austin 1979; Ballentine 1980; Bosart 1981; Bosart and Lin 1984; Riordan et al. 1985; Nielsen 1989; Riordan 1990; Keeter et al. 1995; Riordan 1996). The typical “Carolina” coastal front develops in conjunction with cold air damming and is characterized by an inverted trough in the sea-level pressure field, a tight low-level thermal gradient, and a wind shift (Figure 2.4).

The coastal front can serve as the focus for primary or secondary cyclogenesis that subsequently can affect the entire east coast of the United States, or at other times it can

serve as the focus for the development of severe convective storms in the Carolinas (Vescio et al. 1993). Unfortunately, current numerical forecast models are unable to forecast certain details of these coastal front and cold air damming events (Forbes et al. 1987; Bell and Bosart 1988; Keeter et al. 1995; Riordan 1996). Due in part to a lack of vertical resolution, current numerical models will depict the warm-advection, which occurs over the shallow cold air wedge, as extending to the surface. Thus a forecast of rain is indicated when, in fact, a freezing rain event occurs. Also the temporal and spatial limitations of the current upper-air observational network, consisting of soundings taken only at 12-h intervals, at stations scattered hundreds of kilometers apart, impacts the accuracy and resolution to which these events can be depicted by numerical models (Keeter et al. 1995). Most mesoscale models, and particularly operationally run ones, have only a rather crude representation of the Appalachian Mountains, which further limits the ability of the models to maintain CAD once it occurs.

### **2.3 Retrieving Horizontal Temperature Gradients from Profilers**

With the difficulties in forecasting due to model shortcomings and given the dangerous weather that can occur, improvements are very much needed. This study attempts to use WSR-88D data to obtain additional thermal information during these weather events.

The single-station thermal retrieval technique used here was first proposed by Neiman and Shapiro (1989), where it was applied to VHF wind profiler data. They found the timing, altitude, and magnitude of the profiler-retrieved temperature gradients and horizontal advections compared favorably with synoptic and mesoscale thermal fields and evolutions observed by the operational rawinsonde network. The retrieval of horizontal temperature gradients by a single wind profiler is generally effective in quasi-balanced flow regimes, but becomes less reliable in flow regimes dominated by nonbalanced gravity wave

activity, highly curved flow, or frictional effects. Their technique is adapted to radar winds in this study, and is discussed in Section 4.

Additional studies have been done using wind profiler data and Radio Acoustic Sounding System (RASS) temperature data. Neiman et al. (1991) found temporal fluctuations ( $\sim 3$  h) in the depth of the cold air behind an arctic front that was observed by the RASS between the operational 12-h rawinsonde observing periods, and which agreed with the thermal gradient retrievals from the profiler. Neiman et al. (1992) found mesoscale wind velocity and thermal features up to 400 mb that were unresolved temporally and spatially by the synoptic-scale rawinsonde network. Thermal retrieval techniques using systems that are widely available to NWS forecasters, in particular, the WSR-88D Doppler radars, have neither been developed nor tested. The present study represents the first known attempt to conduct such an investigation.

## **2.4 Velocity Azimuth Display (VAD) Wind Profiles (VWP)**

The VAD display is a graphical plot of mean radial velocity versus azimuth angle for a particular altitude, assuming that the wind is horizontally homogeneous over the scan circle. The geometry of a radar scan used by the VAD technique is shown in Figure 2.5. When the wind is homogeneous at a given altitude, the radial velocity will display a regular sinusoidal behavior as azimuths are scanned by the radar. A best-fit sine wave is compared to the plot of the velocity points if a sufficient number of data points exist. This sine wave is used to compute the wind speed and direction for that particular height. The algorithm then computes the Root Mean Square (RMS) average velocity difference between the data points and the fitted sine wave curve. The RMS gives a measure of the reliability of the estimated mean wind and also may indicate the general level of turbulence and/or non-homogeneity (e.g. the presence of a wind shift associated with frontal passage may invalidate VAD measurements in many cases). The VAD algorithm takes base velocity and

base reflectivity for input, but the base velocity is most important (Crum and Alberty 1993; Klazura and Imy 1993).

The WSR-88D system consists of the radar data acquisition (RDA); the radar product generator (RPG); and principal user processor (PUP). The RDA controls the antenna, collects analog data from the antenna, and converts the analog data to digital data which includes the three basic Doppler radar moments - reflectivity, radial velocity, and spectrum width. The RPG converts the digital data to base products and contains algorithms such as the VAD. The PUP generates the VWP from the VAD and displays the products as fields on a color monitor to the radar observer (Crum and Alberty 1993; Crum et al. 1993).

The VWP is an analysis product available on the WSR-88D Doppler Radar System. This product displays mean horizontal winds (computed from the VAD Algorithm for each level) on a time versus height chart (Fig. 2.6). As many as 30 conventional wind barbs from the surface to 15 km can be plotted every 1,000 ft. (305 m) at 5- to 10- minute intervals. At times, the VWP produces relatively few wind barbs due to the lack of scatterers or when statistical and symmetry errors are exceeded in the VAD processing stage (Klazura and Imy 1993). The VWP winds are normally representative of winds within 20 n mi of the radar. For the heights used in this study (1,000-6,000 ft MSL), the radius of the radar scanning circles used for the VAD were 12-15 km. The VWP is useful in the identification of low- and high-level jets, *inferred* thermal advection patterns (from determination of wind backing and veering), vertical wind shear, *implied* depths of frontal surfaces (from local regions of strong vertical shear), and the development of isentropic lifting situations (*deduced* from synthesis of the above features). It is emphasized that the thermal-related fields are only inferred and not very quantitative. The present research aims to address these operational limitations.

Lee et al. (1994) made a comparison of wind speeds and directions for various heights from VWPs with winds at similar heights from nearby rawinsondes for 12 sites in the

central and eastern United States. The objective was to analyze the VWP product's performance by comparing it with "truth" data. They found that the overall agreement between radar and soundings was very good: at all levels the wind directions differed by less than 10 degrees 85% of the time, whereas wind speed differences were  $< 5$  kt 75% of the time at all levels.

### 3. DATA

Data for this research were collected during the Winter of 1995-1996. This period was chosen because the primary interest was cold air damming. Also, this was the first winter when all seven radar sites in the mid-Atlantic region to be used in this study were operational. Most of the radars did not yet have recorders for saving Level II data, so the analog Level IV data had to be collected as the event took place. The radar data were gathered for the seven sites from the PUP at the Raleigh WSFO. During the two cases which are presented here, the Raleigh radar went down near the end of both events, cutting off data collection from all radar sites, since data from the other six sites was obtained by a callable modem from Raleigh.

Surface and upper air data were the other key data collected. North Carolina State University has a meteorological data ingest system which acquires data from Unidata. These data were used for upper-air analyses, surface analyses, and soundings. Due to a system problem, data were lost for the January 6-7, 1996 case. Information was filled in as much as possible with hand analyses from the Raleigh WSFO and rawinsonde soundings from the National Climatic Data Center (NCDC). WSI, Inc. radar composites were also collected from the internet.

#### 3.1 Rawinsonde Data

Data were gathered from five rawinsonde stations (Fig. 3.1). Since the VWP's are height referenced and the data needed to be in pressure coordinates (for reasons explained in section 4.1), these rawinsonde sites were used to convert the VWP wind data at constant height levels to pressure coordinates using the hypsometric equation (Holton 1992) given as:

$$p_2 = p_1 \exp\left(\frac{z_2 - z_1}{-H}\right), \quad (3.1)$$

where  $p_2$  is the pressure corresponding to the VWP height  $z_2$ ,  $H$  is the scale height ( $R\bar{T}/g$ ), and  $\bar{T}$  is the average temperature which was taken as an approximate layer average ( $z_1$  to  $z_2$ ) on the sounding.

Only two of the radar sites were co-located with rawinsonde sites: INS (Morehead City, NC) and FCX (Blacksburg, VA). The other radars had to be referenced (for the purpose of height to pressure conversion) to the nearest available rawinsonde site: AKQ (Wakefield, VA) with WAL (Wallops Island, VA), ILX (Wilmington, NC) with MHX (Morehead City, NC), CAE (Columbia, SC) with CHS (Charleston, SC), and RAX (Raleigh, NC) and GSP (Greenville/Spartanburg, SC) with GSO (Greensboro, NC). VWP analyses that were performed between sounding releases (every 12 hr) referenced sounding data that were linearly interpolated in time.

### 3.2 VWP Data

Radar data were gathered and archived as the events occurred. VWP data were lost only a couple of times from radars when the communication lines failed for a short period. The other limiting factor for the radar data occurred whenever a fairly clear region moved over one of the radar sites and the lack of scatterers caused the data to be missing. This occurred less than 10% of the time for the two cases in this research.

On the individual VWPs, if one vertical wind level was missing, then it was linearly interpolated from the wind above and below that level. If two or more adjacent data levels were missing, then they were left as a gap in the data. Out of the 1119 wind values used, only 16 were interpolated (~ 1.5%). The winds on a VAD are color coded by the algorithm indicating the root mean square error (rmse) (Fig. 2.6). Only winds with  $\text{rmse} \leq 4$  kt were used as valid wind measurements (for this study, that included ~99% of the wind measurements). Winds were only analyzed for heights  $z \leq 6000$  ft MSL (1.8 km). This was done to make the amount of data processing reasonable, and because this would allow



a full examination of typical depths of cold air comprising CAD events in the mid-Atlantic region (Bell and Bosart 1988).

The focus in this study was to determine changes in thermal fields that occurred over time intervals  $\geq 3$  hr. Since the instantaneous VWP winds might not be representative of the larger trend, average winds were calculated for four stations using 1, 3, 5, 7, and 9 time samples ( $\Delta t \sim 6$  min) for the averaging. Stations used for this test were Raleigh, Greenville/Spartanburg, Wakefield, and Wilmington on December 19, 1996 at 0600 UTC. Levels up to 6,000 ft were used in the time averages. The  $\sim 1$  hour average of 9 samples was considered to be the most representative of the overall wind field. The purpose of the test was to find the minimum amount of data that would still give a good approximation of that same wind field. The differences from the 9-sample for four stations were averaged together at each time and plotted for both wind speed and wind direction. Differences as high as 4 kt resulted for the instantaneous (single sample) wind, whereas for the 3-sample average, that difference drops to  $< 1$  kt (Fig. 3.2a). The wind direction difference was as high as  $8^\circ$  for the instantaneous sample, whereas the 3-sample average displayed differences  $< 5^\circ$ , and there was no significant improvement by adding more samples in the average (Fig. 3.2b). For these reasons, a 3-sample average was used throughout this research for obtaining winds from the VWPs.

### **3.3 Mesoscale Model Data**

The Raleigh NWSFO and North Carolina State University are cooperatively running and using the Mesoscale Atmospheric Simulation System (MASS) model for real-time experimental forecasting (Kramer et al. 1996). MASS is a 3-dimensional, hydrostatic, primitive equation model (Kaplan et al. 1982; Manobianco et al. 1994; Manobianco et al. 1996). The one-way interactive, 15 km resolution nested grid covering the Carolinas and Virginia is used for comparison in this research. The nested simulation is initialized by the

coarse grid (45 km) 12-hour forecast, and is integrated for 24 hours ending concurrently with the 36 h large scale simulation. The model uses a Blackadar planetary boundary layer scheme, modified Kuo-Anthes cumulus parameterization to include downdrafts, and explicit microphysical prediction equations (MASS 1994). The coarse grid MASS model is initialized with the National Center for Environmental Prediction (NCEP) Early ETA model 0000Z initialization. The initial moisture field is supplemented by Manually Digitized Radar and infrared GOES satellite data. The model also contains detailed land use, terrain, normalized differential vegetation index (NDVI), and high resolution sea surface temperature data sets (Kramer et al. 1996). The model was run for the events that are presented here, and used for the purpose of verifying sub-synoptic scale thermal structures retrieved from the VWP analyses that were not resolvable from the synoptic-scale NWS rawinsonde observations.

## 4. ANALYSIS TECHNIQUES

### 4.1 Temperature Gradient and Temperature Advection Retrievals

Temperature gradients were retrieved using the geostrophic thermal wind equation (Holton 1992). If it is assumed that the observed winds are geostrophic ( $\mathbf{V} = \mathbf{V}_g$ ) then the geostrophic wind shear ( $\partial \mathbf{V}_g / \partial p$ ) is given by the observed shear ( $\partial \mathbf{V} / \partial p$ ). The thermal wind relationship will then be given, in pressure coordinates, as:

$$\frac{\partial \mathbf{V}}{\partial p} \approx \frac{\partial \mathbf{V}_g}{\partial p} = \frac{-R}{f \bar{p}} \mathbf{k} \times \nabla T, \quad (4.1)$$

where  $\mathbf{V} = i\mathbf{u} + j\mathbf{v}$ ,  $R$  is the gas constant ( $287 \text{ J kg}^{-1} \text{ K}^{-1}$ );  $f$  the Coriolis parameter ( $\sim 10^{-4} \text{ s}^{-1}$ ),  $\bar{p}$  the layer-mean pressure;  $\mathbf{k}$  vertical unit vector; and  $\nabla T = i\partial T/\partial x + j\partial T/\partial y$  is the geostrophic temperature gradient.  $\partial \mathbf{V}/\partial p$  is defined as  $(\mathbf{V}_2 - \mathbf{V}_1)/(p_2 - p_1)$ . By taking the cross product of Eq. (4.1), using vertical finite-differencing (Haltiner and Williams 1980), and rearranging, we get the single-station retrieved temperature gradient  $\nabla_r T$  on a geopotential height surface as:

$$\nabla_r T(z, t) = \frac{f \bar{p}}{R} \mathbf{k} \times \frac{\mathbf{V}[p(z + \Delta z, t), t] - \mathbf{V}[p(z - \Delta z, t), t]}{2[p(z + \Delta z, t) - p(z - \Delta z, t)]} \quad (4.2)$$

As applied herein,  $\mathbf{V}$  in (4.2) is the VWP wind velocity at height  $z$  and time  $t$ ,  $p$  is the pressure at  $z$  and  $t$ ,  $\Delta z$  is the vertical grid length (305 m), and  $\bar{p} = [p(z + \Delta z, t) + p(z - \Delta z, t)]/2$ . We can obtain the magnitude of  $\nabla_r T$  on the height surface from the  $x$  and  $y$  components of  $\nabla_r T$

$$|\nabla_r T(z, t)| = \left\{ \left[ \frac{\Delta T}{\Delta x}(z, t)_r \right]^2 + \left[ \frac{\Delta T}{\Delta y}(z, t)_r \right]^2 \right\}^{1/2} \quad (4.3)$$

Temperature advection was calculated from the retrieved temperature gradients and the VWP layer-mean winds. The VWP layer-mean wind velocity is given by

$$\bar{\mathbf{V}} = \frac{\mathbf{V}[p(z + \Delta z, t), t] + \mathbf{V}[p(z - \Delta z, t), t]}{2}. \quad (4.4)$$

Combining (4.3) and (4.4) to get the equation for retrieved temperature advection as:

$$-\bar{\mathbf{V}} \cdot \nabla_r T(z, t) = -\left[ \bar{u}(z, t) \frac{\Delta T}{\Delta x}(z, t)_r + \bar{v}(z, t) \frac{\Delta T}{\Delta y}(z, t)_r \right]. \quad (4.5)$$

The single-station retrieved temperature gradient vector  $\nabla_r T$ , as addressed by Neiman and Shapiro (1989), can deviate from the actual temperature gradient vector  $\nabla_{ac} T$  when the wind within the layer of interest is not in geostrophic balance. This can be shown and discussed by using the general form of the thermal wind equation (Forsythe 1945):

$$\nabla_{ac} T = \underbrace{\frac{f p}{R} \mathbf{k} \times \frac{\partial \mathbf{V}}{\partial p}}_a + \underbrace{\frac{p |\mathbf{V}| K_t}{R} \mathbf{k} \times \frac{\partial \mathbf{V}}{\partial p}}_b + \underbrace{\frac{p}{R} \frac{\partial}{\partial p} (|\mathbf{V}| K_t) \mathbf{k} \times \mathbf{V}}_c + \underbrace{\frac{p}{R} \frac{\partial}{\partial p} \left( \mathbf{t} \frac{d|\mathbf{V}|}{dt} \right)}_d, \quad (4.6)$$

where  $K_t$  is the trajectory curvature, and  $\mathbf{t} \frac{d|\mathbf{V}|}{dt}$  is the acceleration of the streamline wind component in natural coordinates. By vertically differentiating the vector momentum equation for frictionless horizontal flow, we can obtain (4.6). Natural coordinates are used where  $\mathbf{t}$  is the horizontal unit vector along the flow.

If the flow is frictionless, straight ( $K_t = 0$ ), and unaccelerated ( $d\mathbf{V}/dt = 0$ ), then (4.6) reduces to geostrophic thermal wind balance  $\nabla_r T = \nabla_{ac} T$ , and terms b, c, and d = 0. Vertical gradients of parcel accelerations can cause departures from geostrophic thermal wind balance. A qualitative assessment of these departures follows: when  $K_t \neq 0$  and is constant with height and  $\partial \mathbf{V} / \partial p \neq 0$  then term b  $\neq 0$ . For cyclonically curved flow ( $K_t > 0$ ),  $|\nabla_r T|$  will underestimate  $|\nabla_{ac} T|$ . During anticyclonically curved flow ( $K_t < 0$ ),  $|\nabla_r T|$  will overestimate  $|\nabla_{ac} T|$ , but in both cases the direction of  $|\nabla_{ac} T|$  will be properly estimated. Errors can arise in direction and magnitude when  $\partial(|\mathbf{V}| K_t) / \partial p \neq 0$ , such that term c  $\neq 0$ . In the simple case where  $\partial |\mathbf{V}| / \partial p < 0$ , and  $\partial K_t / \partial p < 0$  (increasing cyclonic curvature and wind

magnitude with height), and uniform wind direction with height,  $|\nabla_r T|$  will underestimate  $|\nabla_{ac} T|$ . In more complicated cases where directional vertical shear (nonuniform wind direction with height) is present, errors can arise in direction and magnitude. Terms a, b, and c, in Eq. (4.6), can be used to obtain the gradient thermal wind equation.

Vertical gradients of wind-speed accelerations must also be considered. When this occurs and term d  $\neq 0$ , the estimation of  $\nabla_{ac} T$  by  $\nabla_r T$  becomes even less reliable. Term d can be on the same order of magnitude as term a for nonbalanced flow regimes (e.g., mountain-induced or thunderstorm-induced gravity waves). This is mainly due to very large  $|\mathbf{V}_g|$  arising from sharp horizontal gradients of pressure (for example, see Bosart and Seimon 1988). In the presence of these errors from term d, the thermal retrieval technique becomes much less effective. Finally, there was no direct measurements of vertical velocities, which can introduce additional errors in the  $\nabla_r T$  calculations when  $\nabla w$  is large.

## 4.2 Temperature and Potential Temperature Reconstruction

Once the temperature gradients were extracted, a method was developed to recover the temperature field on an isobaric surface using a truncated Taylor series expansion of the temperature at a point:

$$T(x, y, z) = T_0(x_0, y_0, z) + \left( \frac{\Delta T}{\Delta x}(z, t) \right) (x - x_0) + \left( \frac{\Delta T}{\Delta y}(z, t) \right) (y - y_0), \quad (4.7)$$

where  $T(x, y, z)$  is the temperature at the desired radar site;  $T_0$  is the temperature at some reference point;  $\Delta T/\Delta x(z, t)$  and  $\Delta T/\Delta y(z, t)$  are the x and y temperature gradients between the points (WSR-88D radar sites), respectively; and  $(x - x_0)$  and  $(y - y_0)$  are the distances between the points. The method was tested at one of the rawinsonde times using the VWP layer that contained 850 mb; i.e., the retrieved ~850 mb temperatures were compared to the 850 mb rawinsonde temperatures for meteorological continuity and soundness.

The temperature retrieval method used the actual sounding temperature at RNK and MHX (linearly interpolated in time between the 12-hourly rawinsonde release intervals) as the temperatures for the closely located radars at FCX and INS (Fig. 3.1); the reconstructed temperatures were then calculated at the three nearest radar sites (AKQ, RAX, and LTX) using the gradients  $\nabla T$  at FCX and INS in (4.7). The rest of the radars were calculated in the order shown in Figure 4.1. Three calculations were done for each radar (except FCX and INS) by using  $\nabla T$  estimates from the 3 different legs of the triangles, and an average was taken to reduce error caused by the instantaneous gradient from any one radar. In 3 cases, the reference radar for the calculation only had 2 calculated temperatures. A 2-temperature average was calculated in order to have a station temperature for the method. This technique was tested by calculating from the radar at FCX (using the rawinsonde temperature from RNK) to the rawinsonde station at GSO and also from the radar at INS (using the temperature from MHX) to RAX, picking up the  $\nabla T$  from RAX, and calculating again to GSO. These calculated temperatures for GSO were then compared to the rawinsonde observed temperature at GSO. Errors were found to be less than 5°C for all calculations made. Although 5°C is a significant difference, typical errors were < 2°C. However, this was a very limited data set, and results should be tested on a much more extensive data base in future studies.

Once the temperatures were retrieved, Poisson's equation (Holton 1992):

$$\theta = T \left( \frac{1000}{p} \right)^{286}, \quad (4.8)$$

was used to calculate the potential temperatures. The temperatures at each  $z$  and  $t$  were taken with the pressure assigned to that level given by the reverse conversion to pressure coordinates (see section 3.1).

The potential temperatures were plotted on time-height charts for each station and analyzed. The 850 mb isotherm analyses were made from the retrieved temperatures. A plot was made of height versus natural log of pressure at each radar for each time, then the height was retrieved that coincided with 850 mb. Next, a height versus temperature plot was made and the temperature was read at the corresponding height for 850 mb.

## 5. CASE STUDIES

Both case studies were chosen because they are wintertime cases, when mountain-induced gravity waves and convection are minimal. Also, because they are wintertime cases, large horizontal temperature gradients and correspondingly large  $\partial V_g / \partial p$  usually found during this time of year make the technique more effective than during the warm season, when the magnitude of  $\partial V_a / \partial p$  (terms b-d in (4.6)) approaches  $\partial V_g / \partial p$ .

### 5.1 December 18-19, 1995

The synoptic situation in this case consisted of a high pressure center located in the Great Lakes region at 0000 UTC 18 December 1995 (18/0000Z) which did not progress any further eastward over the next 24 hours. Although this location was not ideal for classical CAD, it was able to provide a cold northeasterly flow as an extension of the high pressure system occurred from New England southward into North Carolina, and a large area of precipitation maintained the damming. The precipitation developed before any solar heating could take place, giving little chance for the saturated low levels to warm up over the course of the day. Temperatures in North Carolina remained below 5°C over the entire period. Precipitation continued to fall over the entire state through 19 December. The continued diabatic cooling associated with the precipitation and cloud cover helped reinforce the cold dome. The precipitation was occasionally heavy but remained liquid, and no severe weather was reported in the Carolinas.

The synoptic high pressure over the Great Lakes had good upper level forcing from a strongly confluent flow at 500 mb, which acted to anchor the surface high. The ageostrophic transverse circulation associated with a 300 mb jet entrance region, located over the northeastern United States, may also have aided in driving cold air southward. The clearly defined, wedge-shaped surface high pressure ridge was evident in the surface analysis by 18/0300Z, with the northeasterly flow filtering as far south as Alabama. The



cold wedge maintained its deep southerly location for 33h (until 19/1200Z), when warm frontogenesis occurred in northern Georgia and South Carolina in response to an advancing synoptic low pressure system (Fig. 5.1-5.3). The synoptic low moved along a pressure trough from southern Texas into West Virginia over the course of the two days.

A typical coastal front developed with this event around 18/1500Z. After 24 hours, the coastal front had only moved slightly, to a location just west of Wilmington and Cape Hatteras NC, but never progressed any farther inland (Fig. 5.3). The southerly oceanic winds behind the front were relatively strong; however, the weaker northerly flow on the inland side was aided by the diabatic cooling which reinforced the cold air. The warm front that developed in western South Carolina at 19/0900Z (Fig. 5.1b) remained in that same general location throughout the event (19/1800Z, see Fig. 5.3).

Radar VWP data were collected for the period 19/0600Z-19/1800Z. Figure 5.4a shows the retrieved isotherm analysis for 19/1200Z at 850 mb. If we compare the isotherm pattern to that for the 850 mb level upper air analysis (Fig. 5.5a), we can see that the overall pattern of east-west orientation matches very well. The values of the northern isotherms match very well, while those in South Carolina (farthest from the 2 reference stations) appear to be too warm by about 4°C. Comparing Figure 5.4a to the MASS 19/1200Z initialization (Fig. 5.5b), shows some slightly different details. The MASS initialization depicts cold air in western North Carolina, similar to the retrieved isotherm analysis. The MASS isotherms over western North Carolina are oriented northwest to southeast, which is far different than the west to east orientation of the upper-air analysis. This difference is due to the MASS model's much higher spatial resolution and use of a first guess field provided by the NCEP ETA model. The same tendency in the retrieved isotherms to be too warm by 4°C, compared to the MASS initialization, in the southwest portion of the analysis domain is seen. Thus, it can be concluded that since neither the rawinsondes nor the MASS initial fields detected such warm temperatures in South

Carolina, the retrieval technique has a sizable systematic error growth pattern with increasing distance from the reference rawinsonde sites (the error grows with increasing  $(x-x)$ ,  $(y-y)$  in (4.7) measured relative to MHX and RNK in Fig. 4.1).

Despite this systematic error component, it is possible that the time-evolving patterns in the isotherms have considerable value. Notice that 6 hrs later (Fig. 5.4b), the retrieved isotherm analysis for 19/1800Z depicts a warm tongue in eastern North Carolina. The MASS 850 mb forecast could not be used for comparison, because the model did not handle the cold air damming realistically (Kramer et al. 1996): However, the 19/1800Z surface analysis (Fig. 5.3) shows that warming is indeed very evident in eastern North Carolina where the coastal front has pushed inland, and that a cool pool has developed in western North Carolina, most likely because of evaporational cooling and weak upslope flow. These same two features show up clearly on the retrieved isotherm analysis. Even more interesting is the existence of the warm tongue at 850 mb in the retrieved analysis where the observed surface flow indicates the strongest southwest flow of warm air (the southeastern part of North Carolina). Such conditions promote local convective destabilization.

The greatest reliance can be put in the temperature gradient ( $\nabla_r T$ ) and thermal advection ( $-\bar{\mathbf{V}} \cdot \nabla_r T$ ) retrievals, since these do not depend on the use of a rawinsonde reference temperature. Retrieved temperature advection ( $^{\circ}\text{K}/\text{day}$ ) is displayed on time-height cross sections for all seven radars in Figs. 5.6 and 5.7. Warm advection is seen throughout the lower levels of all cross sections which, if above the cold dome, is consistent with typical cold air damming (Bell and Bosart 1988). The warm-advection at 12Z on the 850 mb analysis (Fig. 5.5a) matches well with what is found at the 1.4 km height for Raleigh, Greenville, and Wakefield, while Morehead City and Wilmington show lesser values of warm advection, consistent with the 850 mb analysis. The strong cold advection seen at the upper levels in the Raleigh cross section is not seen in any of the available real time

data. The VWP's show some backing of the winds at that level, but it is slight, so there was cold advection indicated, but not to the strength that was retrieved.

The retrieved isentropic time-height cross sections for all stations are displayed in Figure 5.8 & 5.9. The Raleigh cross section (Fig. 5.8a) has missing data at 19/0900Z. This shows what results when there are not enough scatterers present over the radar to give returns for a completely filled VWP. In almost all cases, the cross sections indicate the cold air and persistent static stability being contained below 1.4 km, which is a typical depth of the cold dome (Bell and Bosart 1988). However, because of the effects of friction as discussed earlier, the lowest level isentropes are strongly suspect. Static stability is indicated at the reference stations, RNK and MHX, and this stability is carried throughout the retrieved cross sections indicating possible bias. There is static instability indicated at the upper two levels for CAE, GSP, and LTX. This could be an indication of instability and possibly convection, or it could just be a bias in the temperature retrieval. There was no evidence of any widespread convection at any time. Since after 19/1200Z the coastal front was drawing close to LTX and INS, the temperature retrieval was taken across the coastal front between stations. This can create VAD errors (non-homogeneous assumption made questionable), and thus the instantaneous temperature gradients may not be valid across these areas (with a front lying between stations).

Despite problems due to friction, bias, and possibly inhomogeneity, internal consistency between retrieved thermal products is good. For example, the strong warm advection shown at 1.4 km for Raleigh and Greenville (Figs. 5.6a and b) match the warm advection indicated on the retrieved 850 mb analysis (Fig. 5.4a) for these same stations. Also, comparisons were done between retrieved temperature advection cross sections and static stability changes deduced from the retrieved isentropic cross sections. At 12Z, the Raleigh advection field (Fig. 5.6a) shows warm advection at mid levels and cold advection at upper levels. The Raleigh isentropic analysis (Fig. 5.8a) shows the upper two levels

nearly adiabatic, which matches the indicated vertically differential thermal advection. By 18Z, the Raleigh advection field shows strongest cold advection at mid levels with lower values at higher levels, which would indicate stabilization in that layer. The isentropic analyses indicates stabilization in that level between 1.1 and 1.4 km. Likewise, the Greenville advection patterns (Fig. 5.6b) show strong warm advection centered at 1.4 km with weaker warm advection at lower levels between 19/12Z and 19/18Z. The Greenville isentropic analyses (Fig. 5.8b) show stabilization occurring between 1.1 and 1.4 km during this time interval, with destabilization aloft. Similar comparisons made at the other sites also suggest such internal consistency.

There were several possible sources of error for this case, as discussed in section 4.2, but calculations were revealed that these errors were not significant. The region was initially dominated by anticyclonically curved flow which would cause the retrieved temperature gradient  $|\nabla_r T|$  to overestimate the actual one  $|\nabla_{ac} T|$  (from Eq. (4.6) term b). Cyclonically curved flow at Wilmington and Morehead City at later times (19/1200Z, see Fig. 5.5b) would cause  $|\nabla_r T|$  to underestimate  $|\nabla_{ac} T|$ . The nonuniform wind direction with height observed could introduce errors in the direction of  $\nabla_r T$  (from Eq. (4.6) term c). An error analysis was done for Raleigh on 19/1200Z to look at magnitudes of terms b and c in Eq. (4.6). Streamline analysis was done at 850 mb and 925 mb to estimate curvature. The magnitudes of both term b and c were found to be  $2^\circ$  and  $5^\circ$  C/day, respectively. These values were an order of magnitude smaller than the typical values of  $\nabla_r T$  for this case, which were  $20^\circ\text{C/day}$ .

The warm advection at the lowest levels, mentioned earlier, might be partly attributed to friction causing strong ageostrophic flow. The Ekman spiral (caused by friction) displays veering winds with height within the boundary layer and can cause the thermal wind to indicate false warm advection (Stull 1994). The surface flow across the damming region is

almost perpendicular to the isobars (Figs. 5.1-5.3) causing the geostrophic assumption and retrieval technique to be violated.

An example of the magnitude of friction compared to Coriolis is shown in Fig. 5.10 for this cross-isobar surface flow. A calculation was done for the magnitude of friction at the 925 mb level over Raleigh for 19/1200Z (this is somewhere between 600-900 m MSL). The results (not shown) reveal that friction was an order of magnitude smaller than the Coriolis force at this level. Thus, frictional effects cause the retrieval technique results for the first two levels to indicate warm advection that may or may not be valid. By the time the 925 mb level is reached, winds are near enough to geostrophic balance for this technique to give reasonable results. The magnitudes of advections are stronger at stations inland compared to the two stations on the North Carolina coast. The cold air was very shallow as southerly winds were observed on the VWP's at the lowest level (305 m), while surface winds were northerly on the North Carolina coast. Frictional effects in this shallow layer near the surface would magnify actual warm advection that may otherwise have been present in the geostrophic flow pattern.

Fig. 5.11 shows two potential temperature profiles from the Greensboro, NC and Wallops Island, VA soundings at 1200Z. The plots show static stability throughout. The dashed lines are the retrieved potential temperature plots for the nearby radar sites at Raleigh, NC (on the Greensboro plot) and Wakefield, VA (on the Wallops Island plot). Both radar site plots show good agreement with the upper air station plots (neither are co-located) above 1,000 m. Large temperature differences are seen in the lower layers (below 1,000 m). This is due to the strong ageostrophic flow in the lower layers, which will be discussed in detail later. The veering of the winds to a southerly direction by  $\sim 0.7$  km MSL indicates the shallowness of the cold dome. The derived analyses emphasize features above this altitude, which was roughly at the top of the cold air.

## 5.2 January 6-7, 1996

The synoptic situation in this case initially was comprised of very cold air over eastern Canada, but a secondary synoptic high pressure center built eastward into the northeastern U.S. very early on 6 January. The advection of the cold air southward was assisted by the density of the cold air to the north and confluent flow at 500 mb. The cold air was in place by the time the precipitation moved across North Carolina from 06/1500Z-07/0900Z. The overall pattern of cyclogenesis showed a classical cold air damming event with very cold and dry surface-based air in North Carolina which was dammed against the Appalachian Mountains. This air mass provided additional cooling from strong easterly upslope flow and diabatic cooling as precipitation evaporated as it fell into the quite dry subcloud layer.

Several short waves were seen at upper levels on the western side of the Appalachian Mountains, which supported multiple surface lows from Tennessee into the Gulf of Mexico at 7/0000Z (Fig. 5.12b). A surface low developed off of the South Carolina coast about 7/0600Z. While not a classical Miller Type "B" cyclogenesis pattern, there were Miller Type "B" characteristics in the form of a commonly shared frontal boundary between the multiple lows to the west and the developing low off of the coast of South Carolina (Miller 1946). The multiple surface lows finally evolved into one dominating single low as the diving upper level jet rotated around the base of the 500 mb trough. The cold air damming coupled with these multiple surface lows meant changing thermal advection patterns and a relatively broad transition zone of mixed precipitation (Fig. 5.15) with multiple precipitation type changes. To give an idea of the precipitation problems, Raleigh reported 2 inches of snow and 2 inches of sleet mixed with periodic glazing from freezing rain for the period of the event. The precipitation gradually ended late on 7 January across North Carolina and the light precipitation that was left fell in the form of snow.

Radar VWP data were collected for the period 06/2100-07/1200Z. Figure 5.16a depicts the 07/0000Z isotherm analysis for the 1.4 km (850 mb) layer. The general pattern

of the isotherms matches with the 850 mb upper air analysis (Fig. 5.16b), though the temperature errors are greatest on the coast (1-2°C). This was due to the fact that INS had no data for this level and so there was no gradient retrieved for the temperature calculations. The temperature retrieval technique outlined is biased when the data is missing for either of the reference stations. Comparison with MASS was not possible for this case, because the model moved the damming out so quickly that comparison could only be made at the initialization time. The initialization time did not coincide with any of the times in this data set.

The RAX (Raleigh) temperature advection cross-section for this case (Fig. 5.17a) shows strong warm advection throughout the period centered at the 1.1 km level. The strongest warm advection coincides with a 50 kt southeasterly low-level jet that was best seen in the VWP at 07/0300Z. The jet does not taper off until 07/1200Z, when the warm advection also shows a decrease in strength. The same advection pattern and VWP jet appear for GSP, but the jet tapers off 07/0900Z. Because of the effects of friction as discussed in the earlier case, the lowest levels give highly questionable results, where warm advection is indicated.

The isentropic cross sections for all stations indicate strong static stability for the entire period after 7/03Z (Fig. 5.19 & 5.20). The depth of the cold air is indicated to be somewhat shallower to the east (LTX and INS), compared to RAX, FCX, and AKQ. This is consistent with classic damming as the depth of the cold air lessens as you move away from the mountains (Bell and Bosart 1988). In almost all cross sections, the vertical isentropic gradient shows increasing stability developed with time in the lower layers. These results are supported by the fact that the coldest surface temperatures occurred at the last data time period (7/1200Z) according to figure 5.14. These isentropic retrievals are suspicious because of the bias discussed earlier.

Internal consistency was again checked and found to be good. For example, the retrieved 850 mb analysis for 00Z (Fig. 5.16a) indicates strong warm advection at Columbia and Raleigh, with weaker warm advection at Greenville and Wakefield. The retrieved temperature advection at 1.4 km height for these stations has exactly those kind of characteristics, with strong warm advection at Raleigh and Columbia (Figs. 5.17a and c), weaker at Greenville (Fig. 5.17b), and very weak at Wakefield (Fig. 5.18a). Also, the strong warm advection at mid levels for Raleigh (Fig. 5.17a) with weaker warm advection above and below would tend to stabilize the lower levels and destabilize the upper levels after 07/00Z. The isentropic analysis for Raleigh (Fig. 5.19a) shows increased stabilization in low levels and decreased stabilization in upper levels for the same period. Finally, the Greenville advection patterns (Fig. 5.17b) show the same warm advection bullseye as Raleigh centered at about 1.4 km. The Greenville isentropic analysis (Fig. 5.19b) again indicates increased stabilization in low levels and decreased stabilization in upper levels after 07/03Z.

Some of the possible sources for error in this case, as discussed in section 4.2, are similar to section 5.1. The region was dominated by anticyclonically curved surface flow which would cause  $|\nabla_r T|$  to overestimate  $|\nabla_{ac} T|$  (from Eq. (4.6) term b). Cyclonically curved flow at Wilmington and Morehead City from 07/0600Z on (Fig. 5.13b) caused  $|\nabla_r T|$  to underestimate  $|\nabla_{ac} T|$ . The nonuniform wind direction with height observed could introduce errors in the direction of  $\nabla_r T$  (from Eq. (4.6) term c).

Given the observed surface cooling that occurred between 07/00Z and 07/12Z, while during the same interval of time, the sea level pressures continually decreased (Figs. 5-12-5.14), an operational forecaster would be perplexed about whether the strength of the CAD event, the depth of the cold air, and the low-level stratification were actually increasing or decreasing. However, the VWP thermal advection and isentropic cross section retrievals



clearly provide much valuable information into these issues concerning the rapidly changing thermodynamic structure of CAD events.

## 6. CONCLUSIONS

A single-station thermal gradient retrieval technique and thermal fields reconstruction has been applied to wind profile data obtained from WSR-88D VWP. Single-station time-height cross section displays of temperature gradient, thermal advection, and isentropes were produced at seven radar sites across the Mid-Atlantic region. Thermal fields were then retrieved from the seven stations and mapped as isotherms on the 850 mb surface. These products were then compared against currently available analysis products (surface analyses, upper air analyses, and the NCSU MASS mesoscale model fields). The retrieval method was applied to two cold air damming events in the winter of 1995-1996.

Thermal fields compared favorably with other analyses for key aspects of warm and cold advection through these CAD events, except in lowest levels (below 0.7 km MSL) where ageostrophy caused by friction gives poor results. Of special note is the way the technique, in the cross sections, was able to characterize the changing strength of the advectons. Also, the internal consistency between the different retrieved products was very good. Comparison of vertically differentiable advection and stabilization changes were found to be largely consistent. These new products can provide details about the vertical structure of thermal fields and advection patterns at hourly intervals (though only 3-hourly analyses were produced here), compared to the 12-hr interval analyses that are available from the operational rawinsonde network.

Some limitations in retrieving these thermal fields are the need for scatterers (usually hydrometeors) over the radar to provide a useable VWP, and the need to pressure reference the VWP data to retrieve the thermal fields. This method is very cumbersome to manipulate by hand, because converting the VWP analog plots into digital data with accuracy took a great deal of time and was subject to  $\pm 5$  kt,  $\pm 10^\circ$  errors. Also, radar down time can take away data access, or cause sites to be missing. Some of this limitations and problems can be adjusted for in the future. Problems remain due to the effects of friction and non-

homogeneity over the VAD scanning circle, but calculations suggest that errors arising from curvature and other non-geostrophic effects were generally negligible, at least in the two cases studied here.

This technique needs to be tested on other cold air damming events, and also to the onset and decay periods of CAD when more ageostrophic flow typically exists. The technique should also be used on other types of weather events. In the future, it may be possible to directly obtain digital values of the VWP winds for both direction and speed from the WSR-88D RPG product generator. Indeed, this will be required if this technique is ever to have any hope of ever being implemented and tested operationally. A way of checking for vertical consistency should be built into the technique, to avoid superadiabatic lapse rates which occurred sometimes at higher levels. An objective method for obtaining the temperature values (which does not require referencing rawinsonde sites) is needed, perhaps using mesoscale model forecasts.

If the retrieval method continues to prove useful, this process could be built into a WSR-88D algorithm, and these products could then be generated on the PUP. This information could provide much needed information to forecasters in the future. It is very important to develop techniques like this, that take advantage of the new technology already in place.

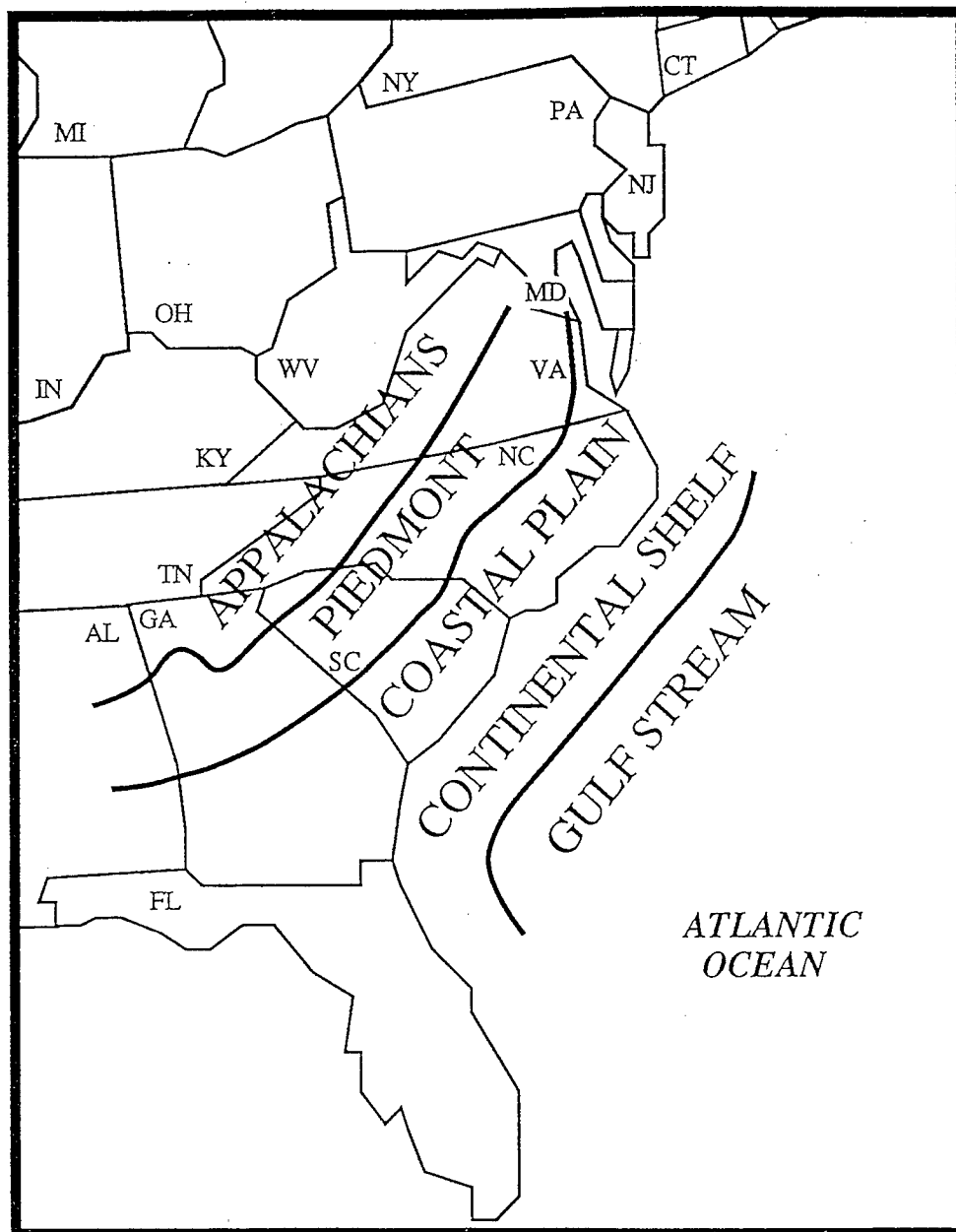


Figure 2.1. Topography of the southeastern United States (Dirks et al. 1988).

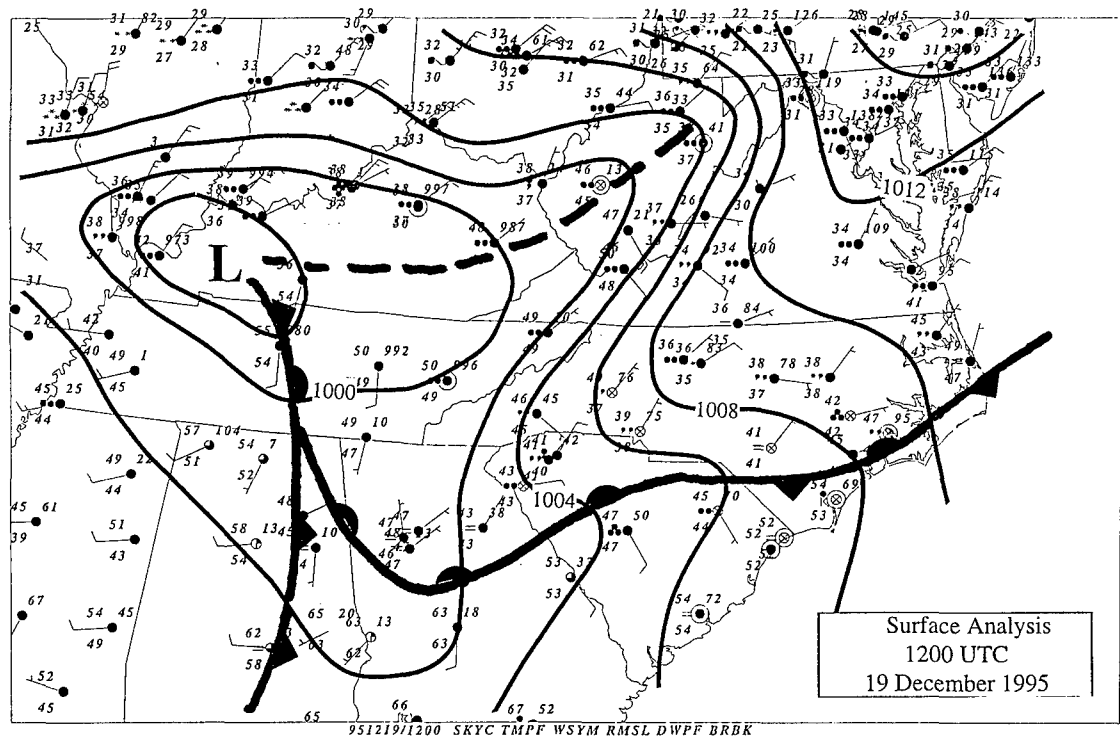


Figure 2.2. Surface frontal analysis for 19 December 1995 at 1200 UTC. Thin solid lines are isobars every 2 mb. The “U”-shaped isobars over Virginia and the Carolinas indicate cold air damming.

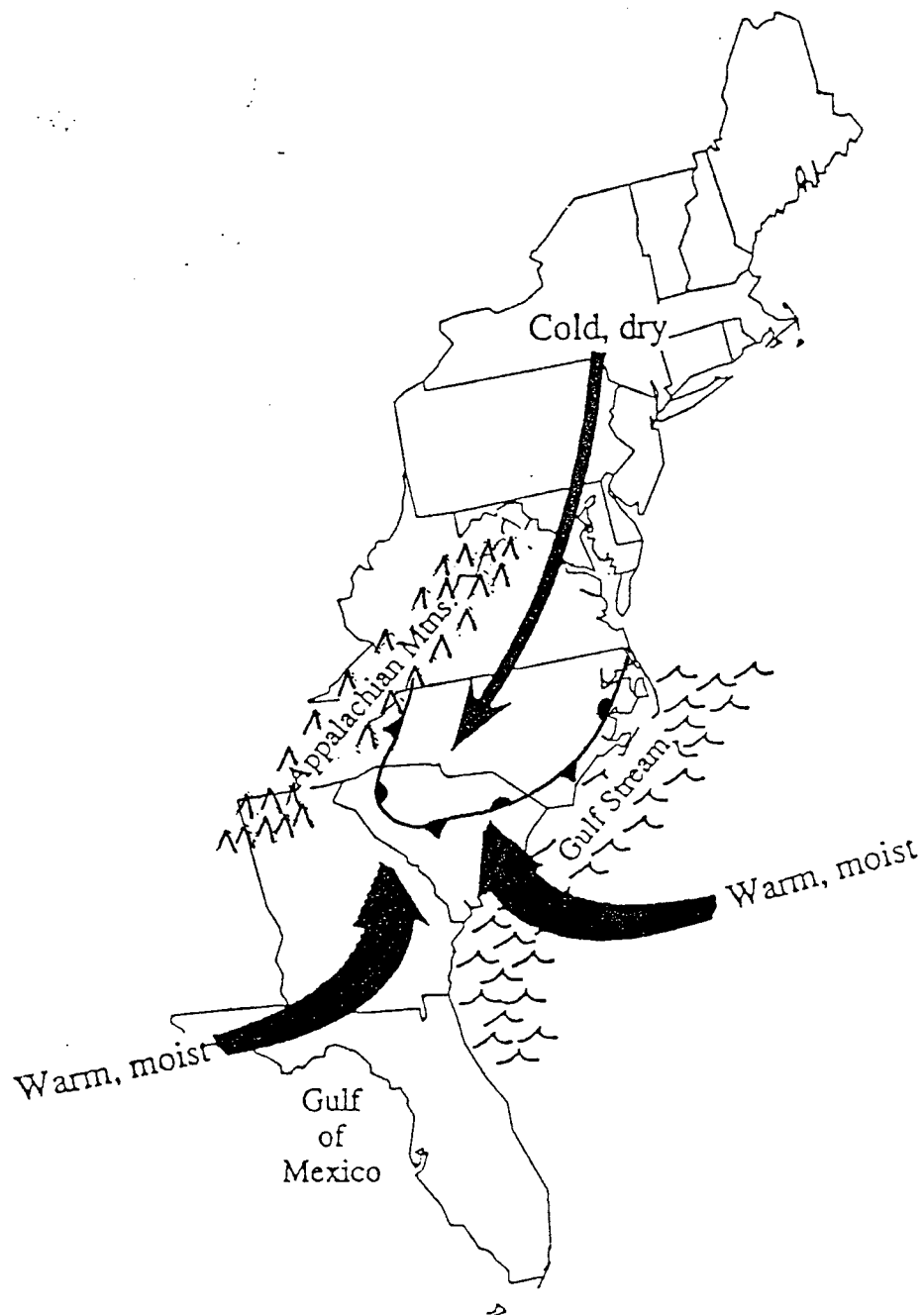


Figure 2.3. Typical flow pattern associated with cold air damming events in the Carolinas and Virginia (adopted from Souza 1994).

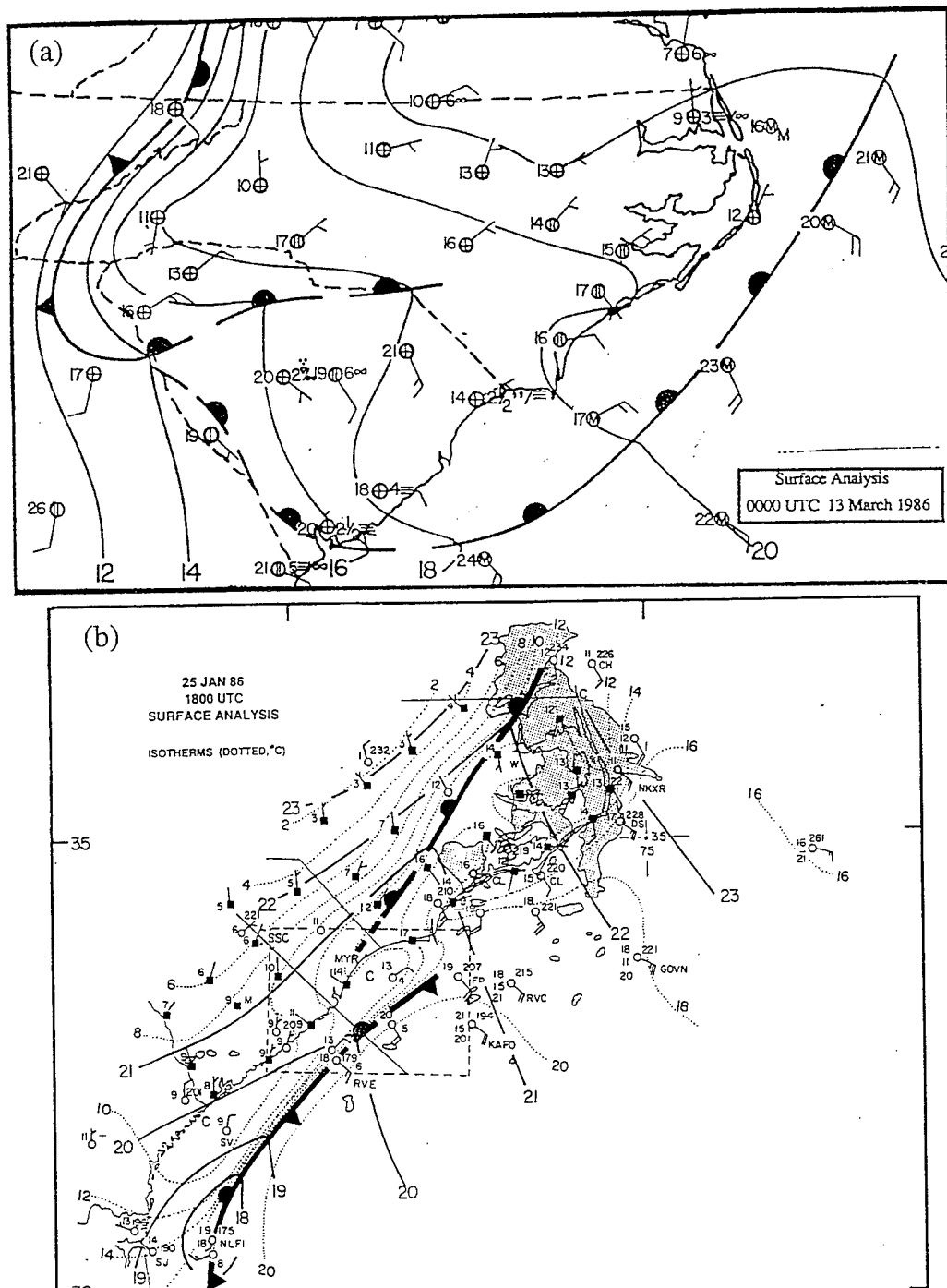


Figure 2.4 a) Mesoscale surface analysis for 13 March 1986 at 0000 UTC (Bauman 1989). Thin solid lines are isobars (12 = 1012 mb) every 2 mb. b) Mesoscale surface analysis for 25 January 1986 at 1800 UTC (Riordan 1990) showing tight coastal front isotherm gradient and radar-observed precipitation.

## Velocity-Azimuth Display

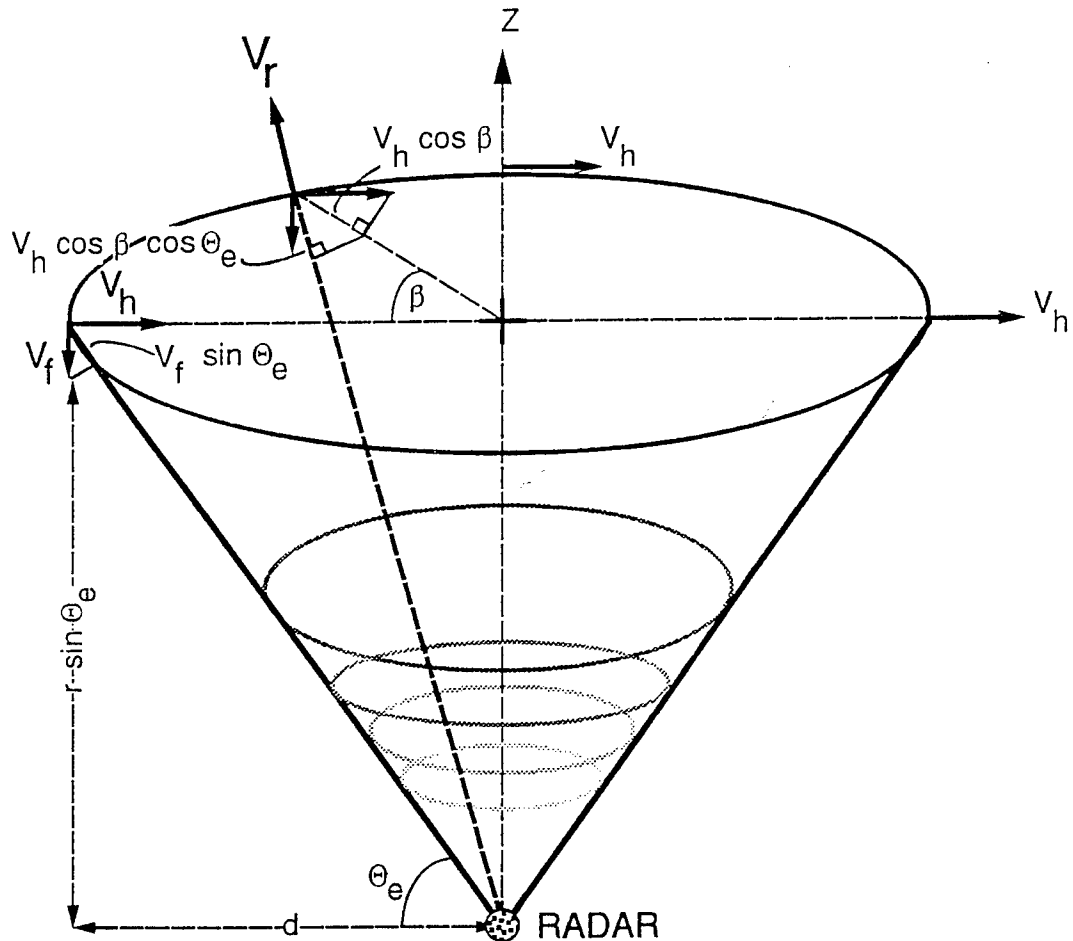


Figure 2.5. Geometry of scan for wind measurement by VAD technique (Crum et al. 1993).  $\theta_e$  is the radar elevation angle,  $V_r$  is fall velocity,  $V_h$  is horizontal velocity,  $V_r$  is the velocity toward or away from the radar,  $d$  is horizontal distance from radar to scatterer,  $r$  is the range to scatterer along the beam, and  $\beta$  is the angle between horizontal wind direction and radar beam.



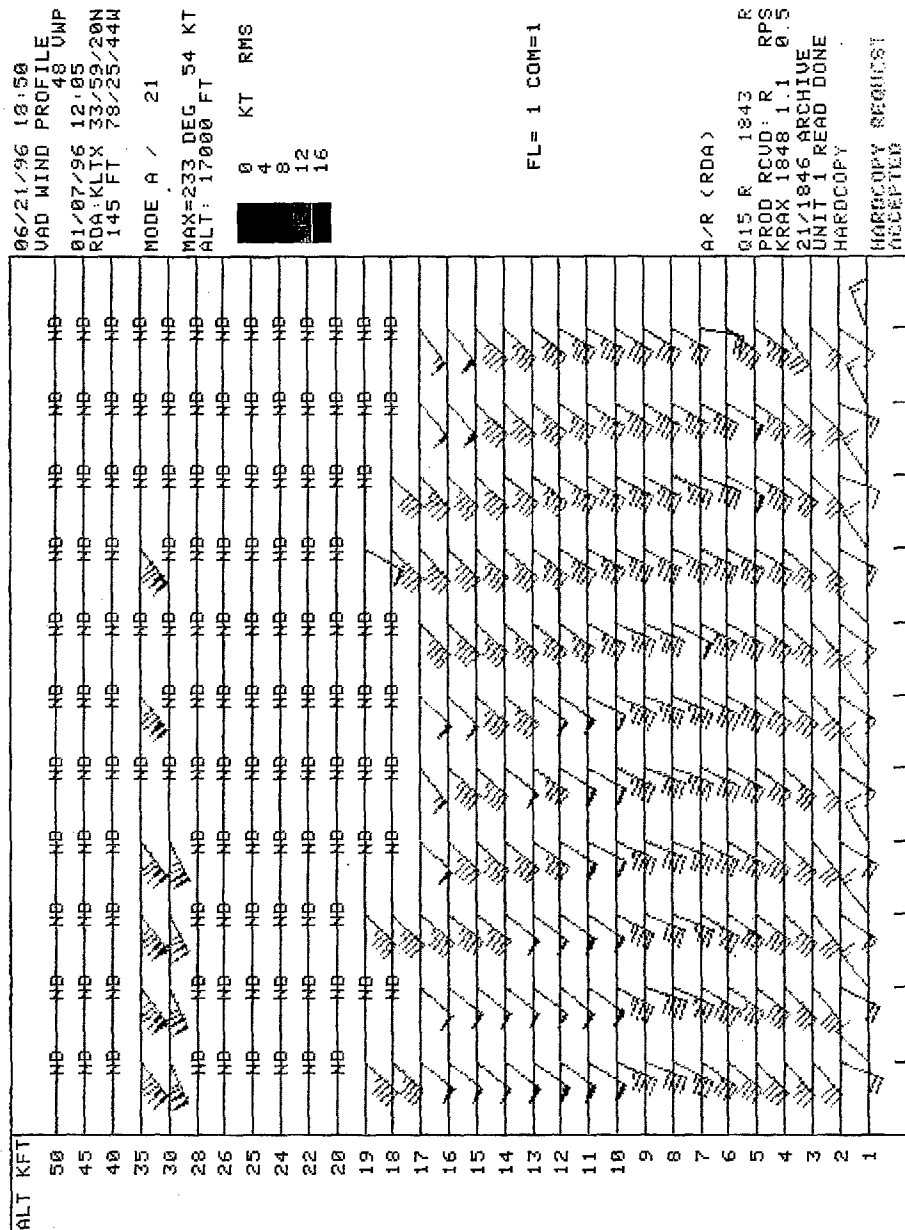


Figure 2.6. WSR-88D VAD wind profile for Wilmington, NC on 7 January 1996 at 1205 UTC. Standard wind barbs are plotted in knots. Height is on left in 1,000 ft. increments. Time increases to the right in 6 minute increments. The wind RMS error is color coded according to legend on the right.

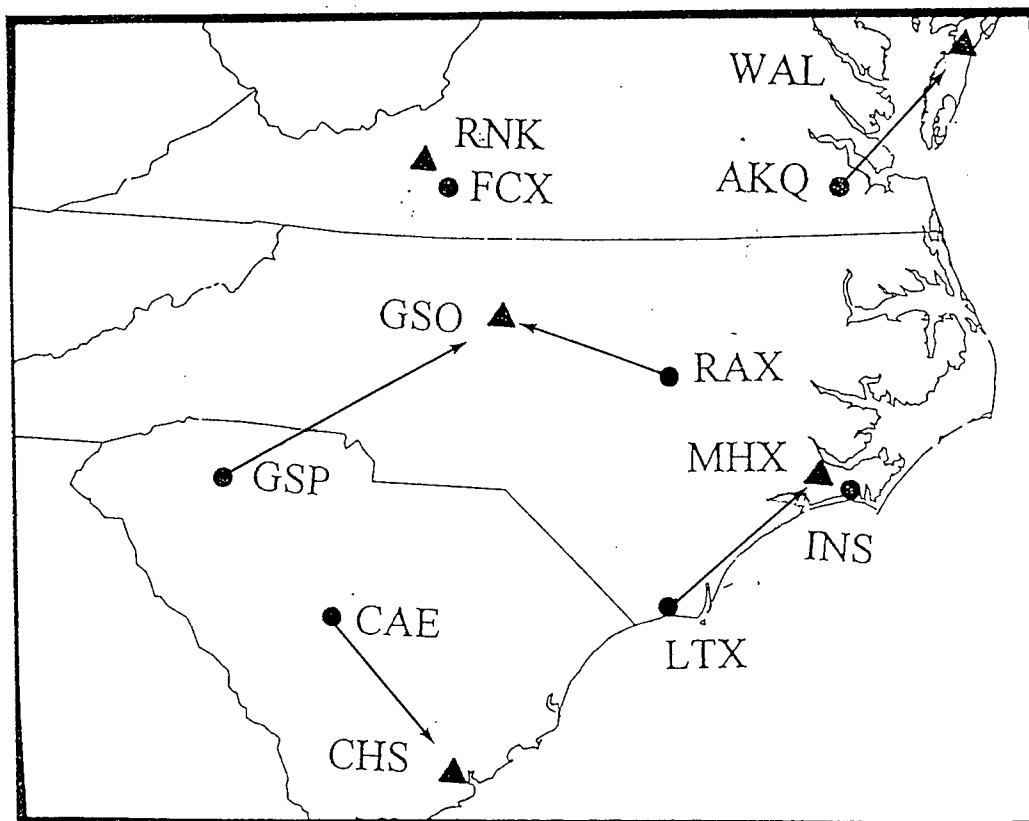


Figure 3.1. Mid-Atlantic region showing the stations used in this study. Dots indicate WSR-88D Doppler Radar sites and triangles are rawinsonde sites. RNK is Roanoke, FCX is Blacksburg, WAL is Wallops Island, GSO is Greensboro, RAX is Raleigh, MHX and INS are Morehead City, GSP is Greenville/Spartanburg, CAE is Columbia, CHS is Charleston, and LTX is Wilmington. Arrows indicate to which rawinsonde site the radar sites were referenced.

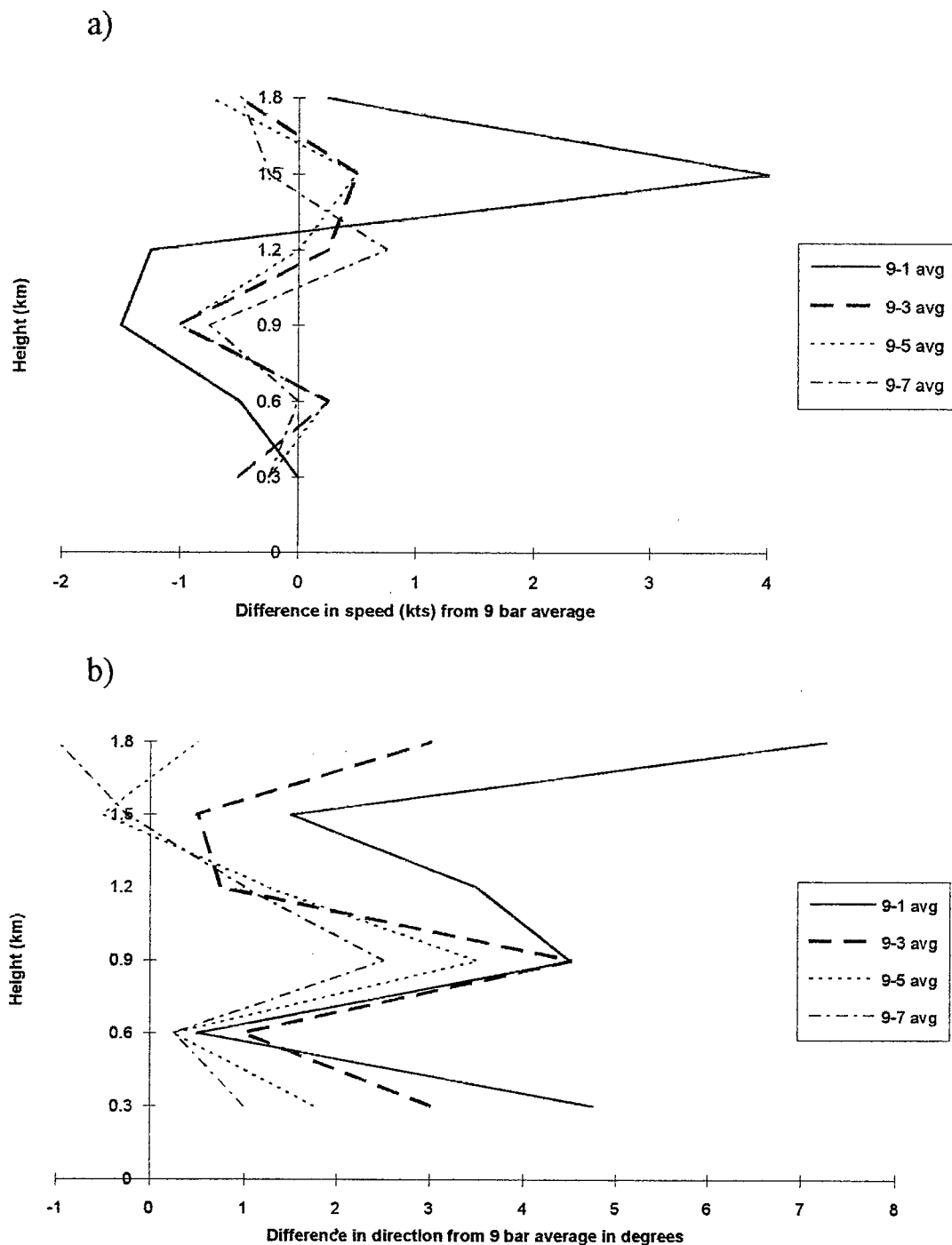


Figure 3.2. Error analysis of time sampling technique for (a) VWP wind speed and (b) VWP wind direction. Legends are on figure. 9 time sample averages (9 sets of winds averaged for each height) were used as the baseline for comparison. 1, 3, 5, and 7 time sample averages were then figured and subtracted from the 9 bar average for both speed and direction. Size of errors from subtracting other time averages from the 9 bar time average are shown across the bottom. Each plot is the 9 bar time average minus the sample average shown in legend.

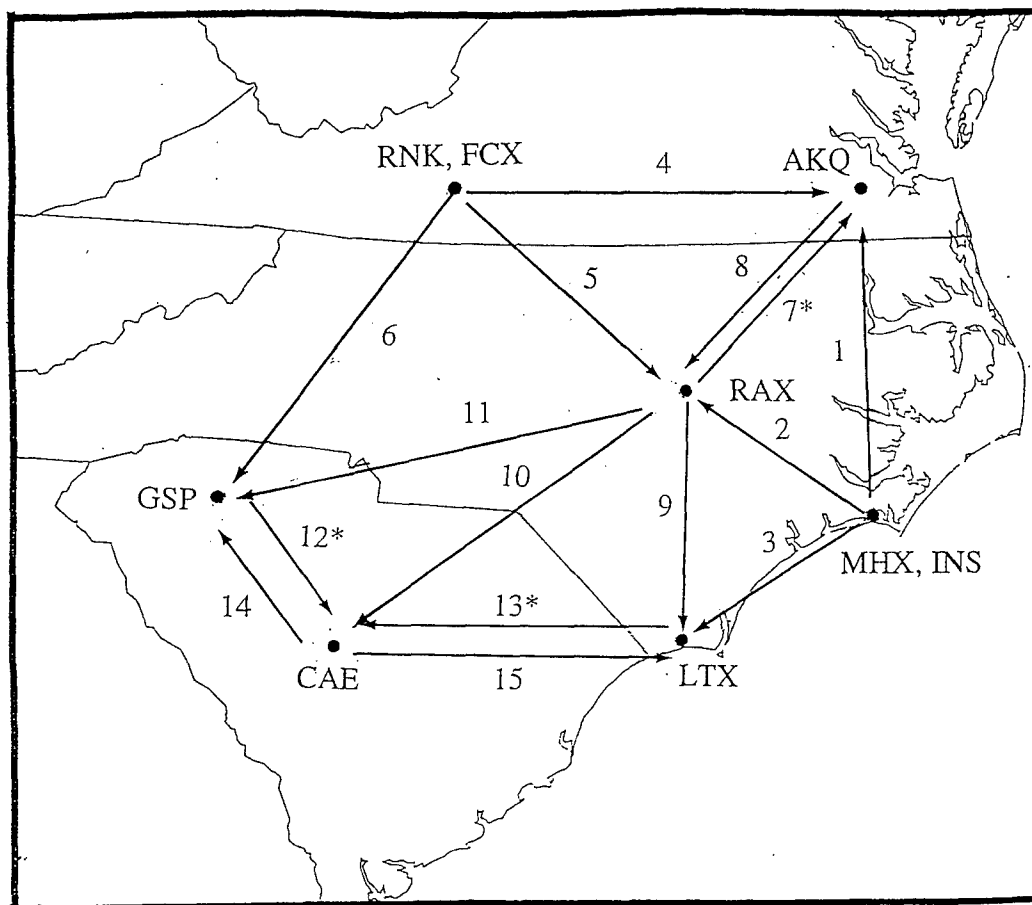


Figure 4.1. Diagram showing sequential order of temperature calculations. Arrows point from station used as reference point to the station for which the temperature was being calculated. \* indicates calculations done with a two temperature average. (e.g. 7\* means that the calculation from RAX to AKQ was done with the temperature at RAX averaged from two calculated temperatures.)

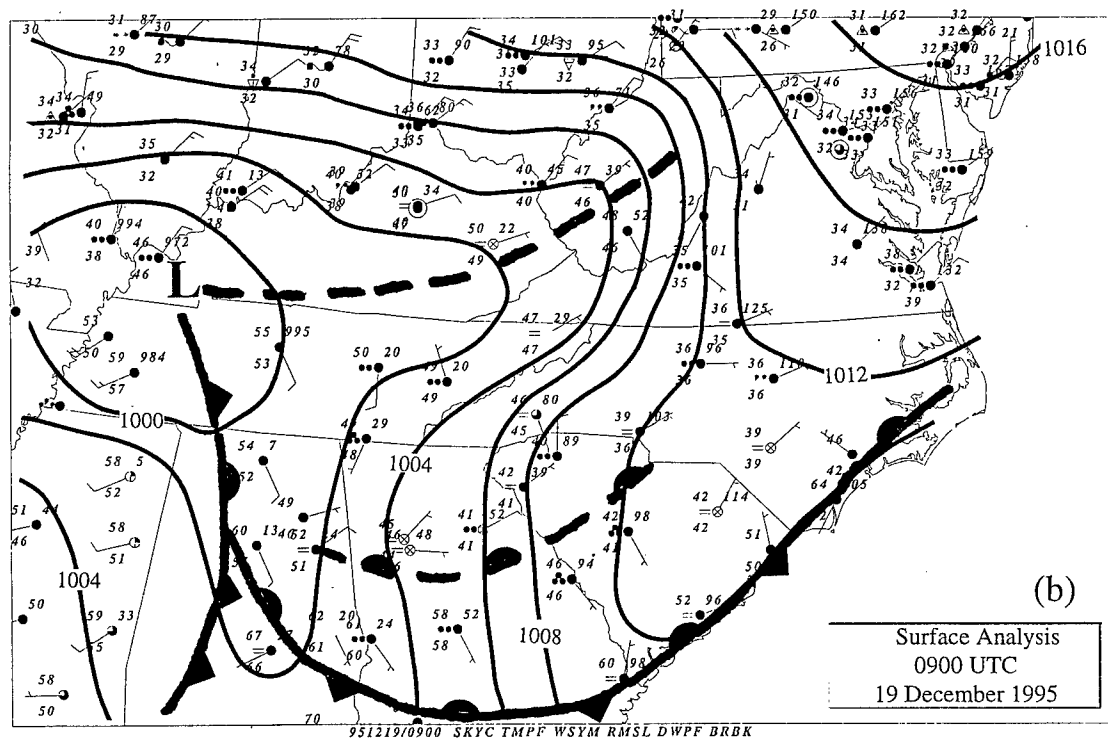
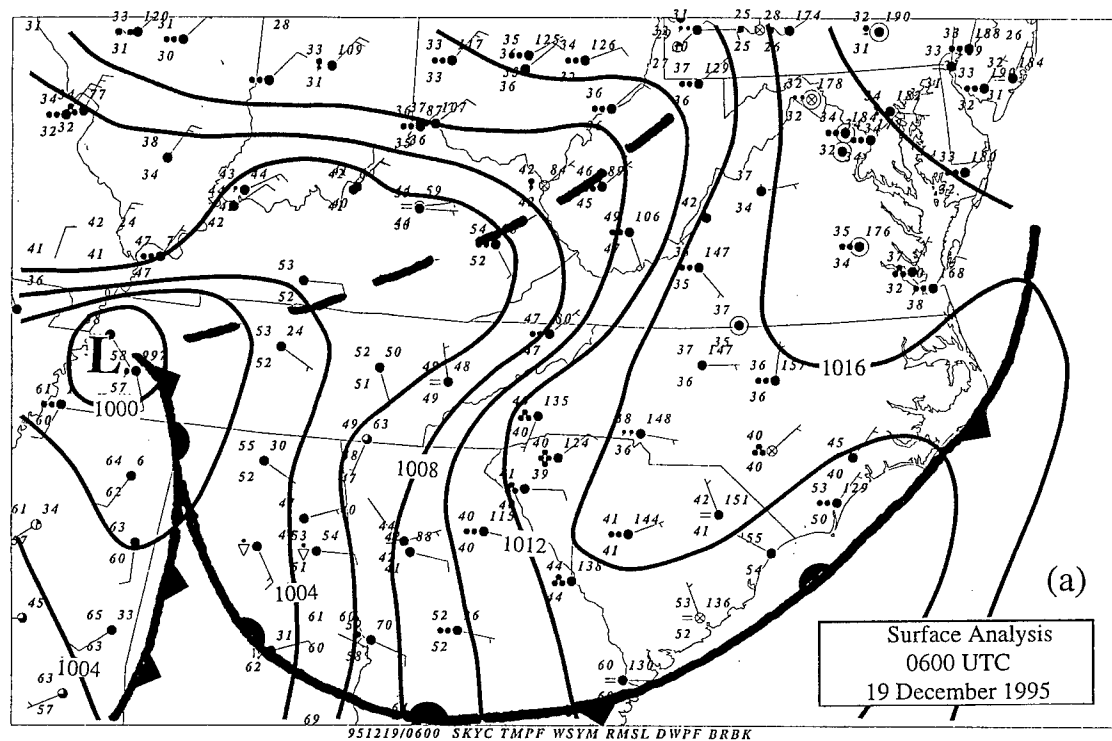


Figure 5.1. Surface analysis for 19 December 1995 at (a) 0600 UTC and (b) 0900 UTC. Thin solid lines are isobars every 2 mb.

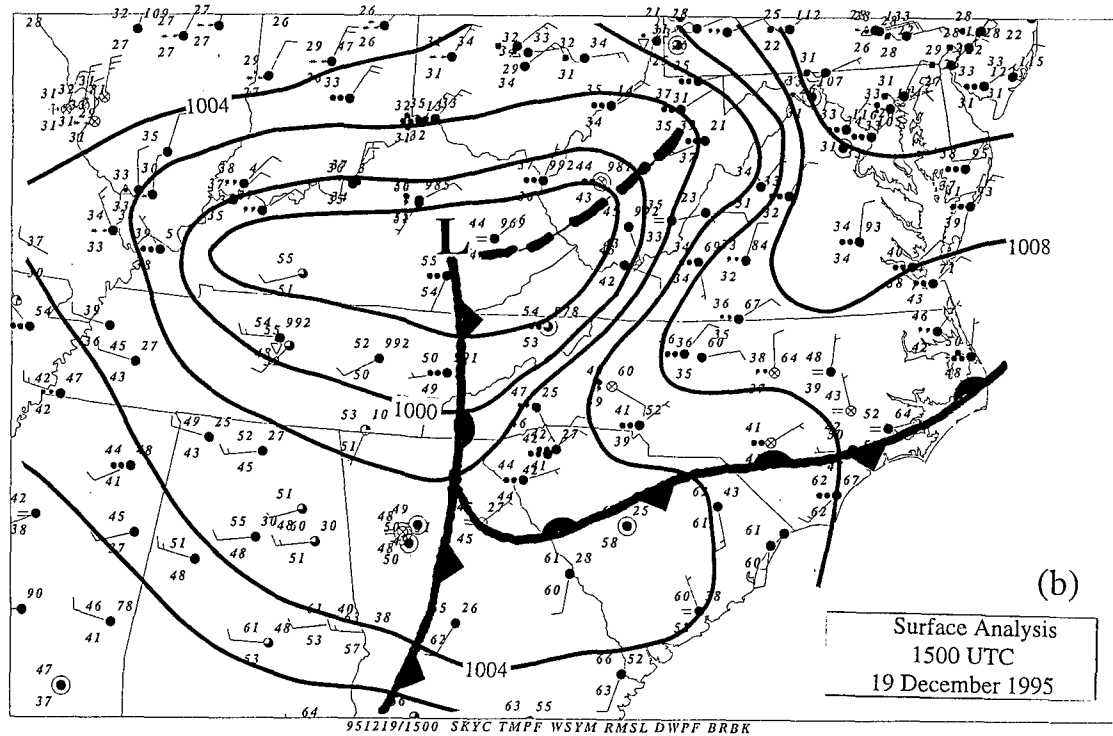
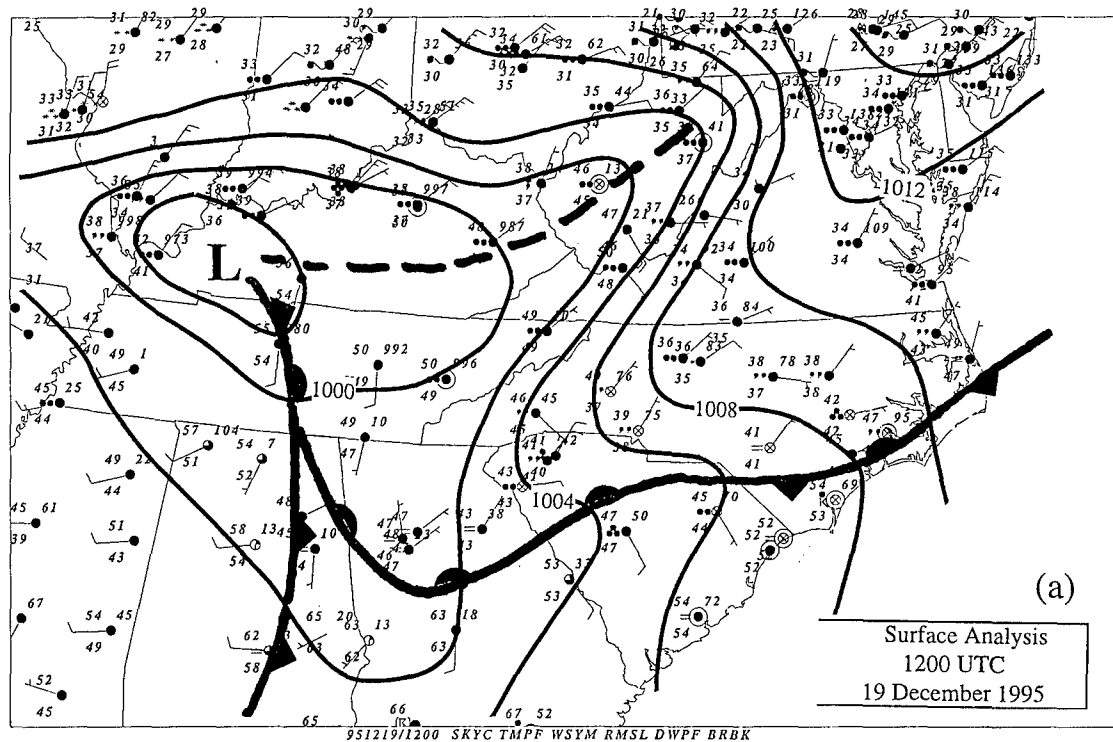


Figure 5.2. Same as Fig. 5.1 except for (a) 1200 UTC and (b) 1500 UTC.

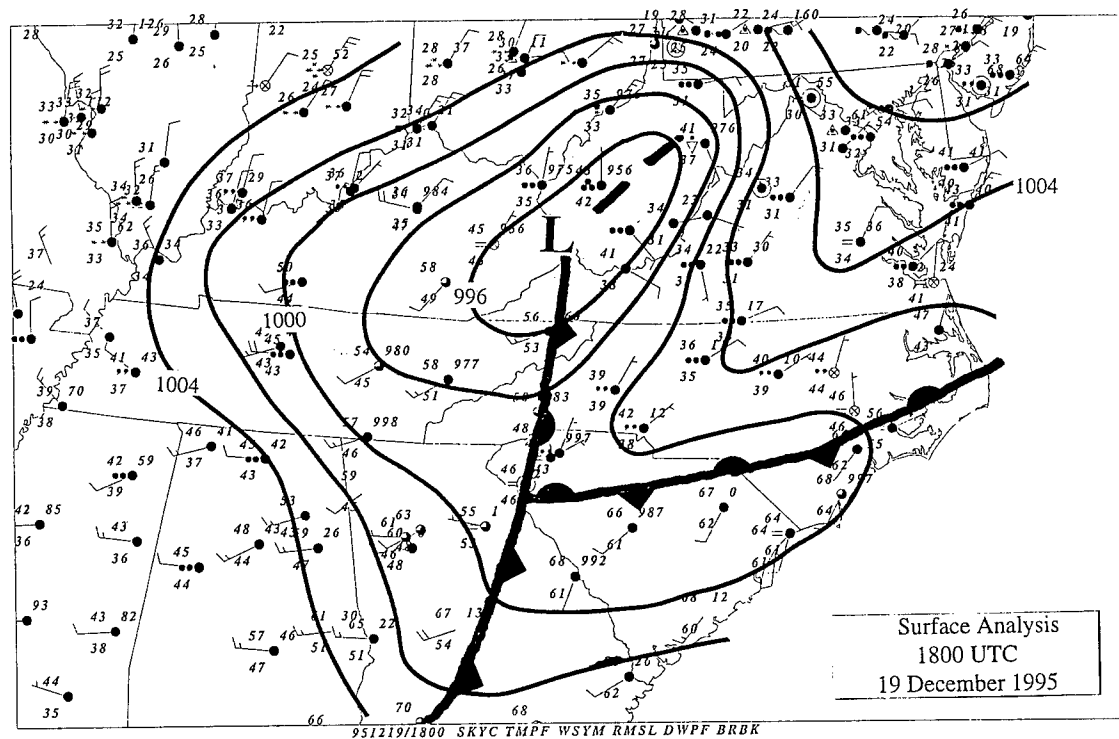


Figure 5.3. Same as Fig. 5.1 except for 1800 UTC.

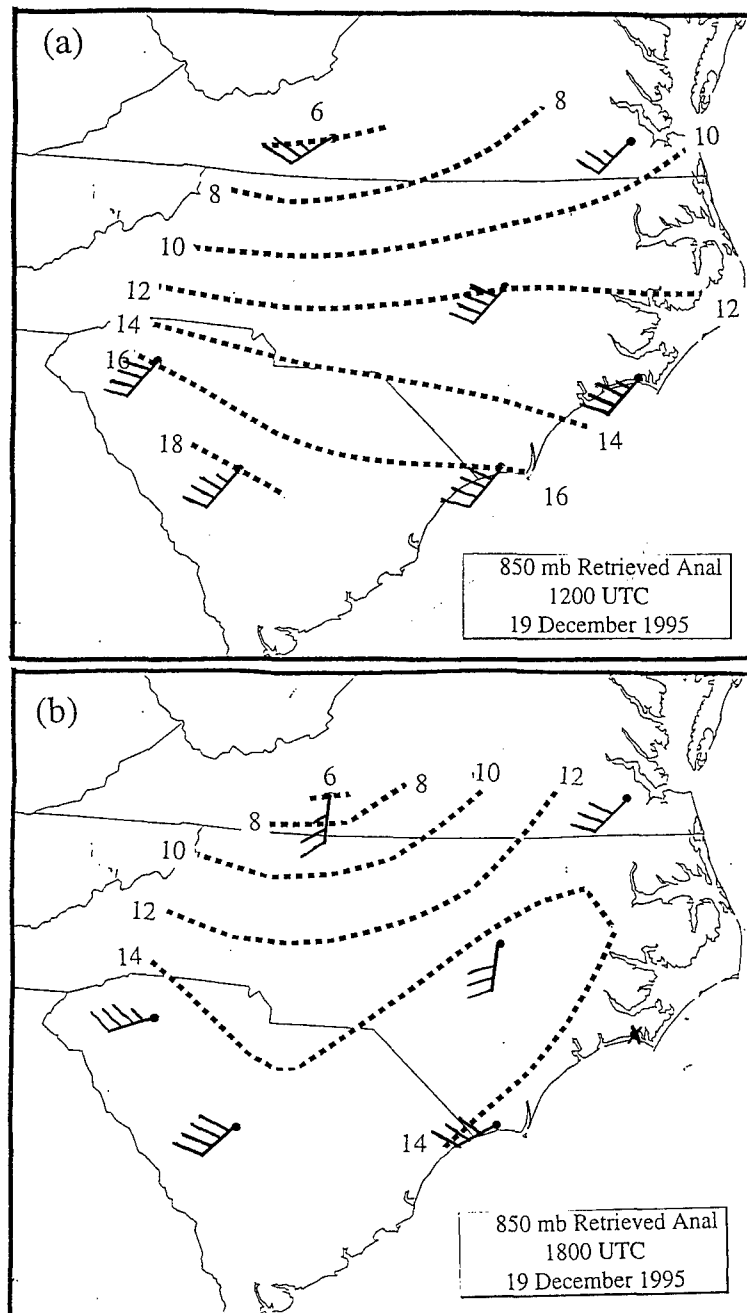


Figure 5.4. 850 mb analysis of retrieved temperature. Dashed lines are isotherms every 2°C for 19 December 1995 at (a) 1200 UTC and (b) 1800 UTC. Winds (kts) represent VWP winds at 850 mb.



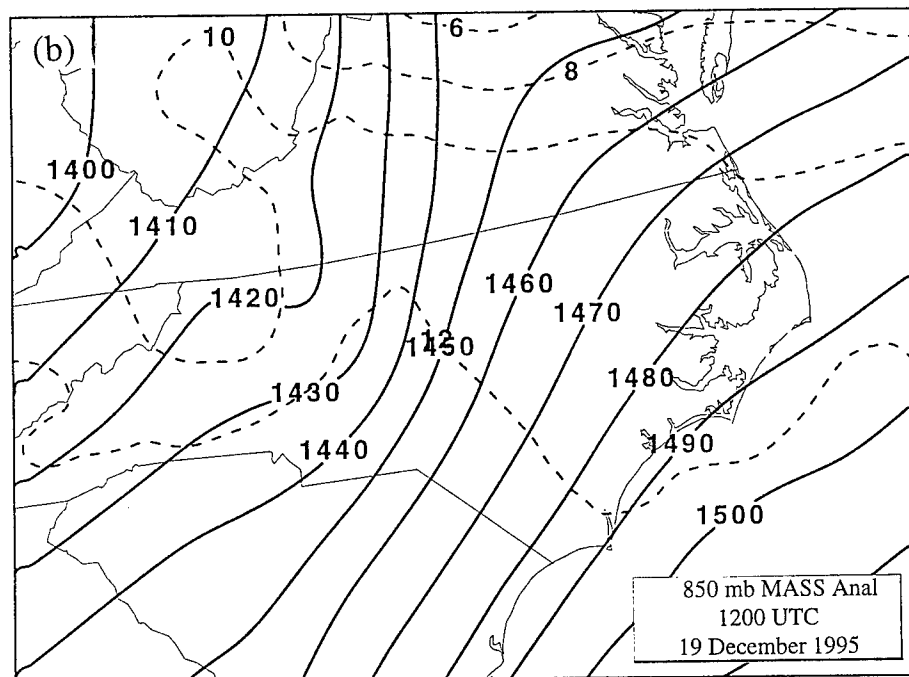
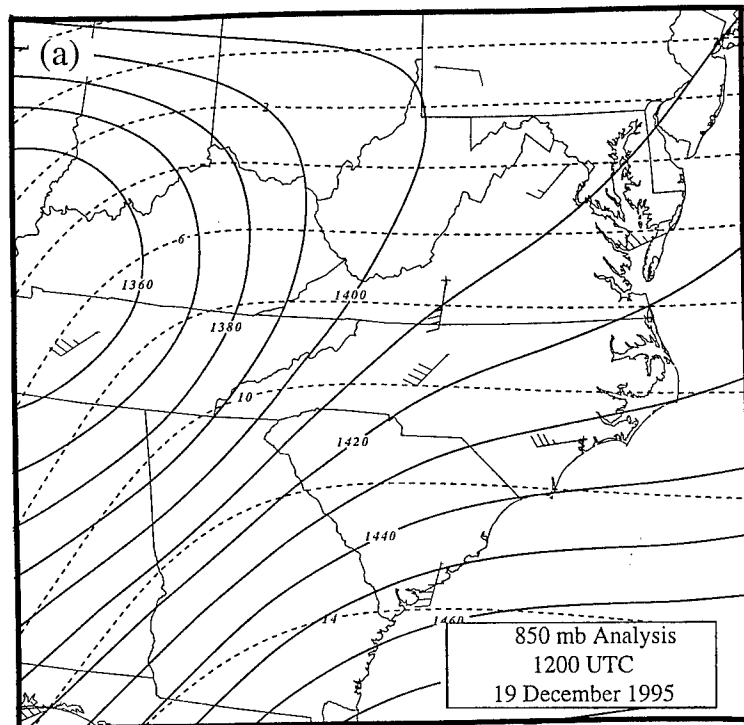


Figure 5.5. a) 850 mb analysis for 19 December 1995 at 1200 UTC. b) MASS model 850 mb initialization for 19 December 1995 at 1200 UTC. Thin solid lines are height contours every 10 m and dotted lines are isotherms every 2°C.

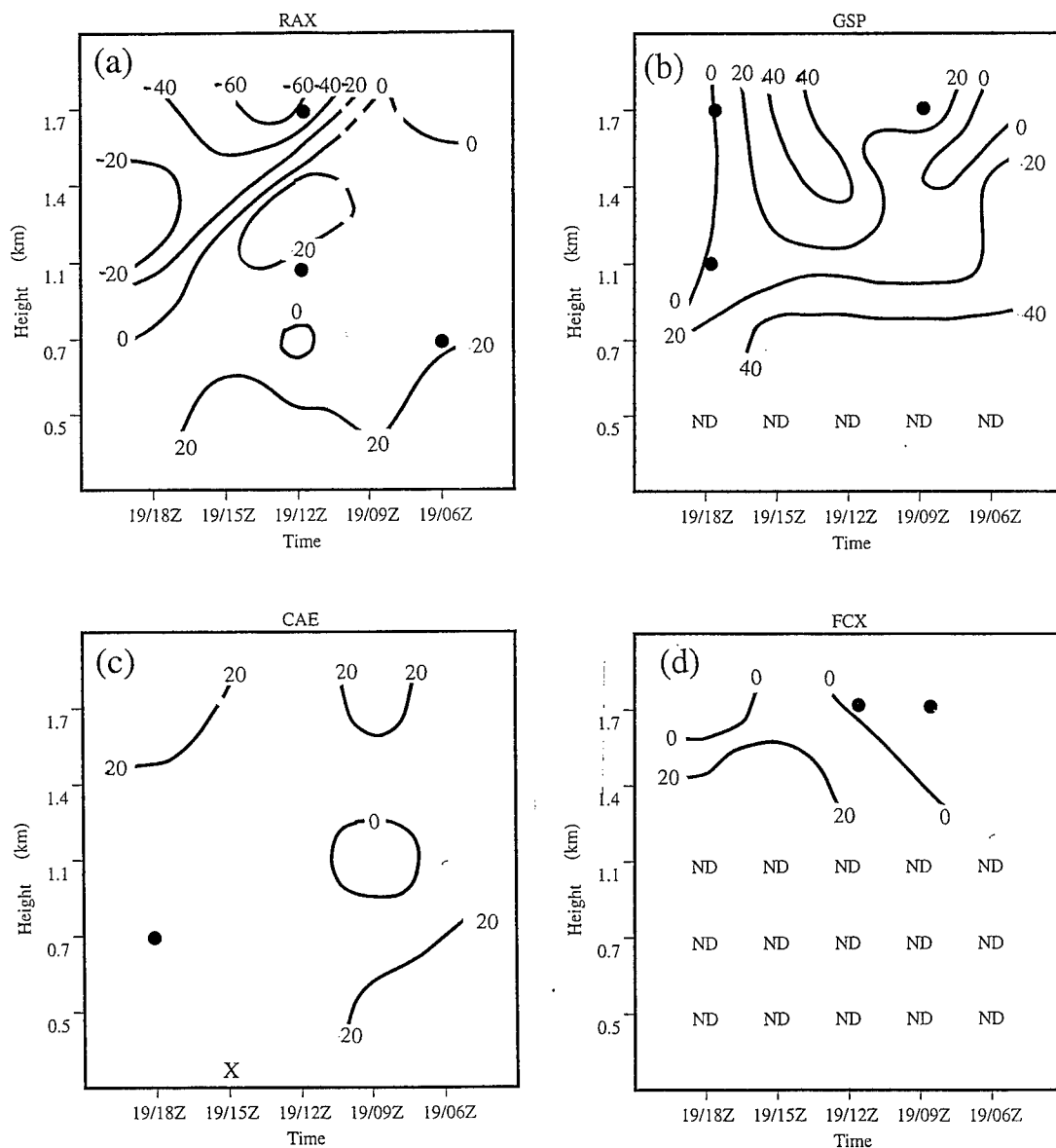


Figure 5.6. Temperature advection time-height cross sections for 19 December 1995. a) Raleigh, NC, b) Greenville/Spartanburg, SC, c) Columbia, SC, and d) Blacksburg, VA. Solid lines are temperature advection intervals of 20°C/day (positive = warm advection). Dashed area indicates interpolation for a missing point during analysis. A dot indicates vertical interpolation of data point on VVPs. An X over a time period indicates all data missing for that time. ND means no data at that level (below ground). Heights on left are MSL.

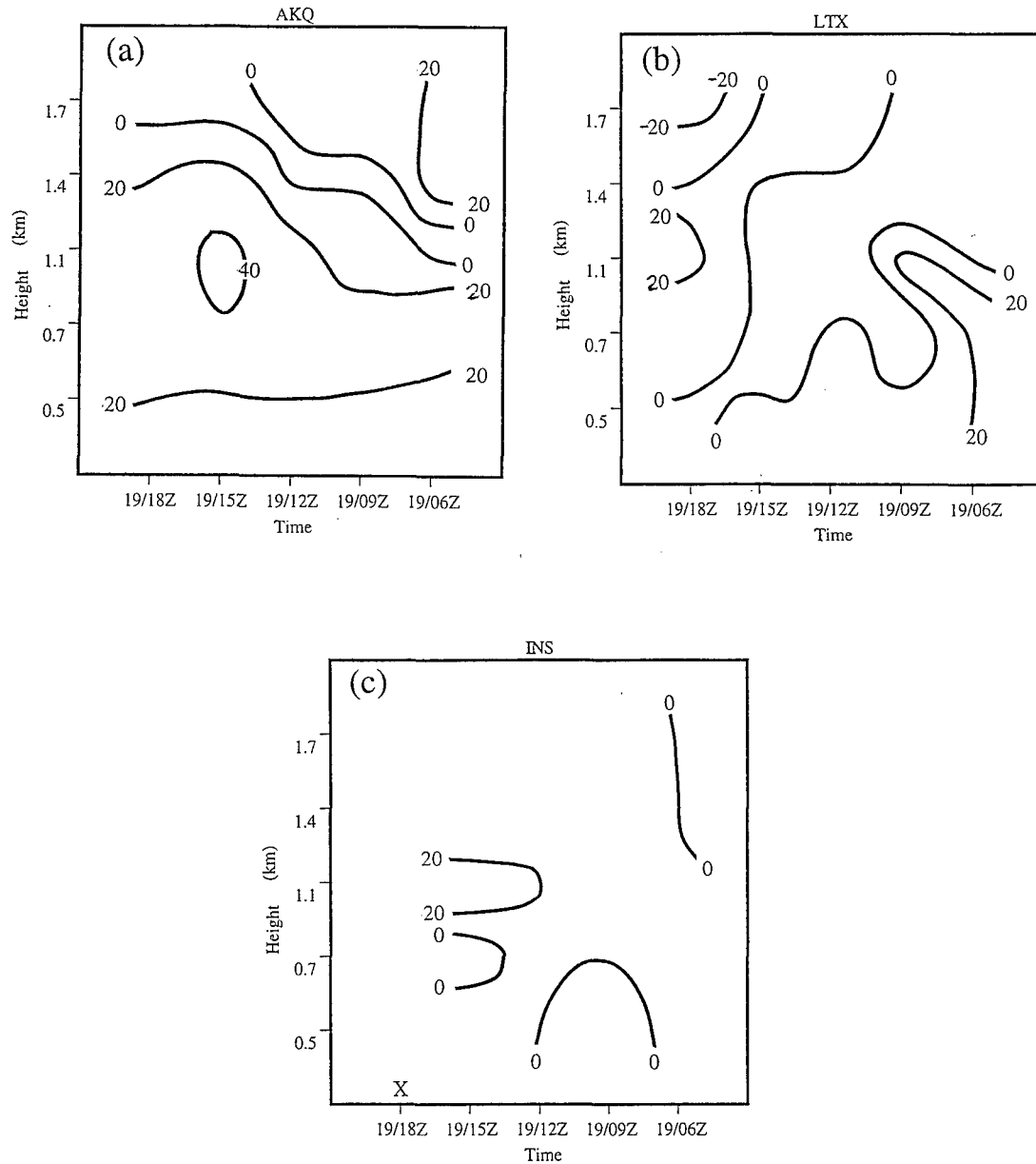


Figure 5.7. Same as Fig. 5.6 except for a) Wakefield, VA, b) Wilmington, NC, and c) Morehead City, NC.

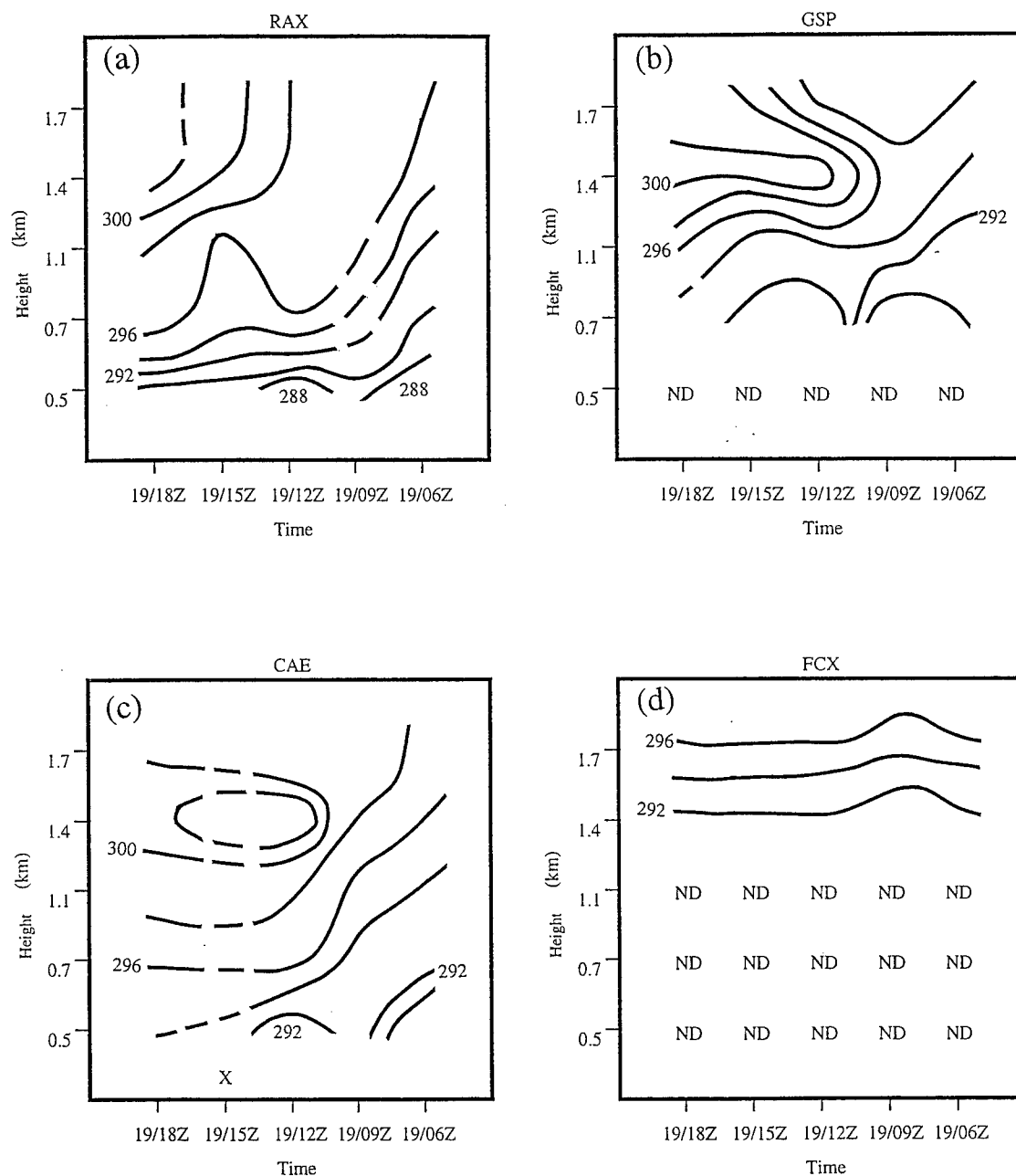


Figure 5.8. Isentropic time-height cross sections for 19 December 1995. a) Raleigh, NC, b) Greenville/Spartanburg, SC, c) Columbia, SC, and d) Blacksburg, VA. Solid lines are isentropes every 2°K. Dashed area indicates interpolation for a missing point. An X over a time period indicates all data missing for that time. ND means no data at that level (below ground). Heights on left are MSL.

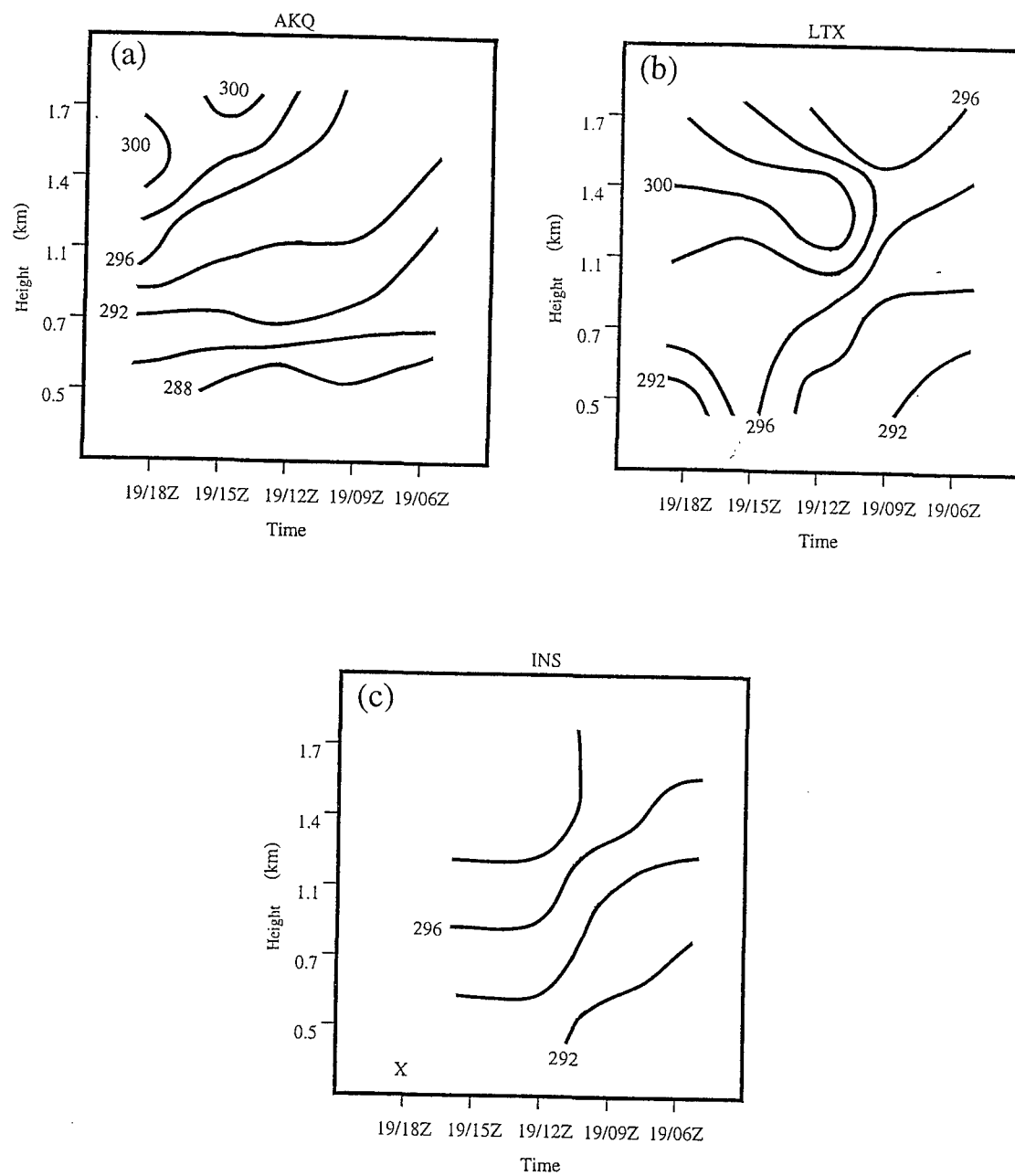


Figure 5.9. Same as Fig. 5.8 except for a) Wakefield, VA, b) Wilmington, NC, and c) Morehead City, NC.

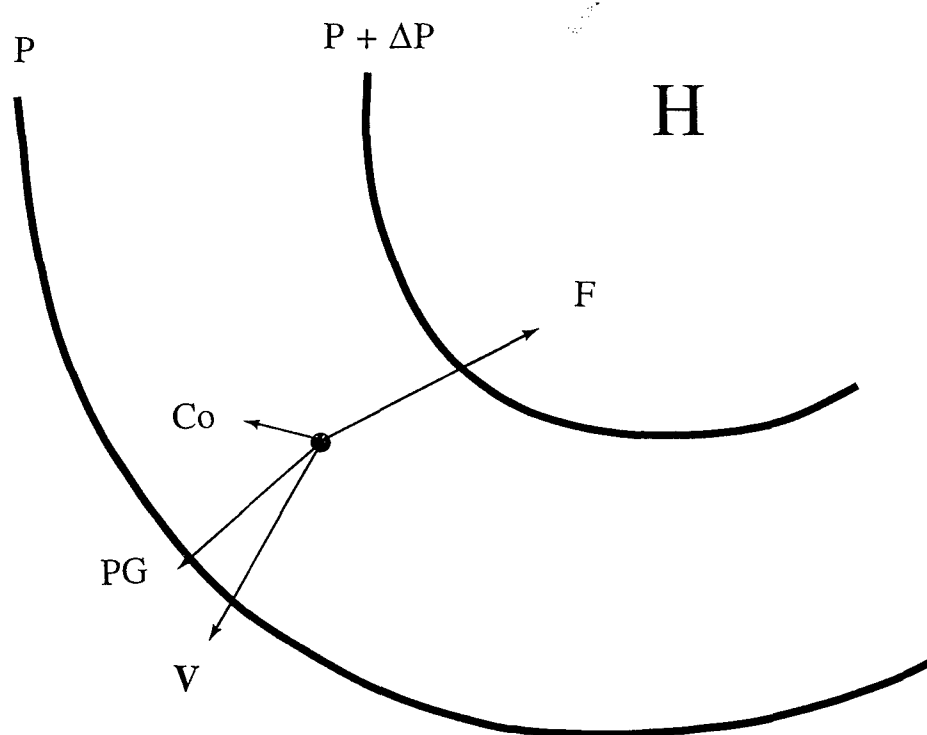


Figure 5.10. Balance of surface flow in CAD event with strong frictional effects.  $V$  is observed wind,  $PG$  is pressure gradient force,  $Co$  is coriolis force,  $F$  is friction, and solid lines are isobars.

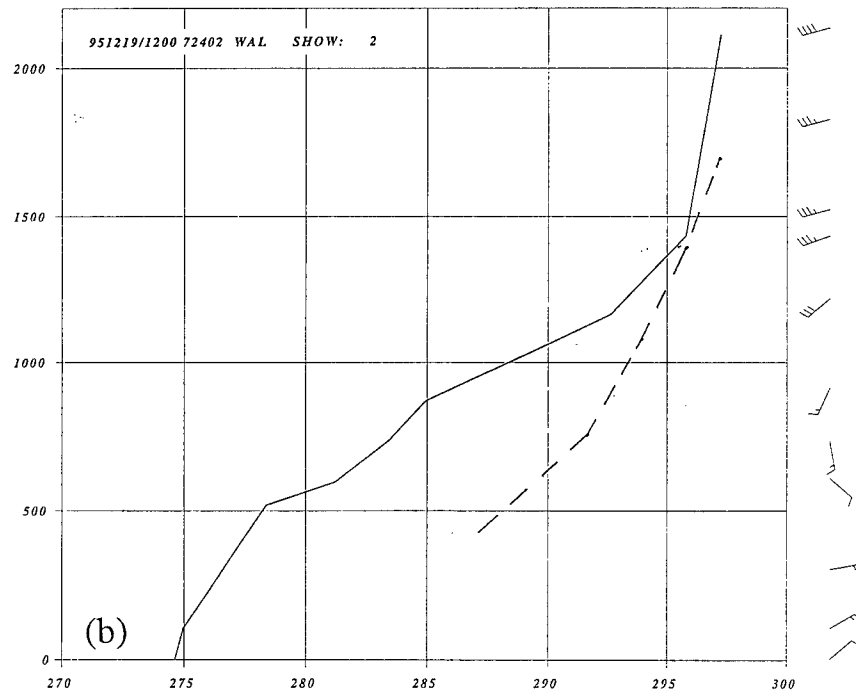
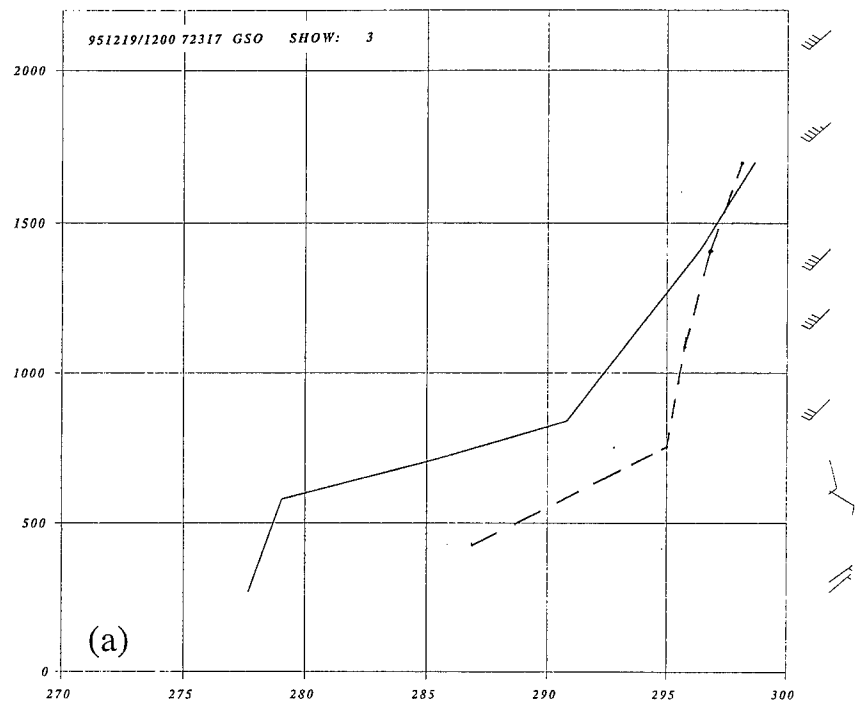


Figure 5.11. Potential Temperature plots for 1200 UTC 19 December 1995. Height is on the left in meters MSL. Solid lines are potential temperature ( $^{\circ}\text{K}$ ) derived from rawinsondes at (a) Greensboro, NC and (b) Wallops Island, VA. Dotted lines are radar retrieved potential temperatures for (a) Raleigh, NC and (b) Wakefield, VA.

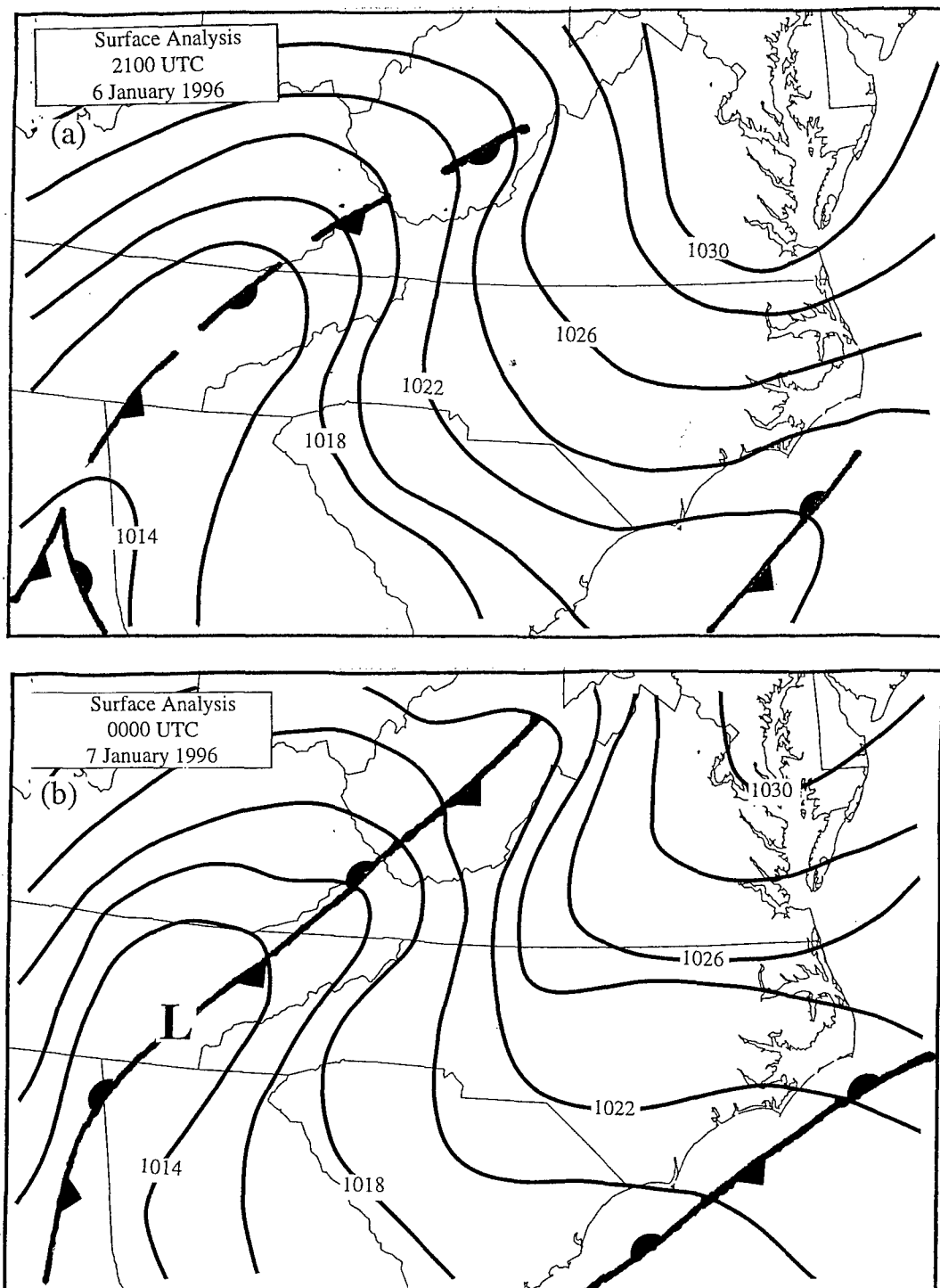


Figure 5.12. Surface analysis for (a) 2100 UTC 6 January 1996 and (b) 0000 UTC 7 January 1996. Thin solid lines are isobars every 2 mb.



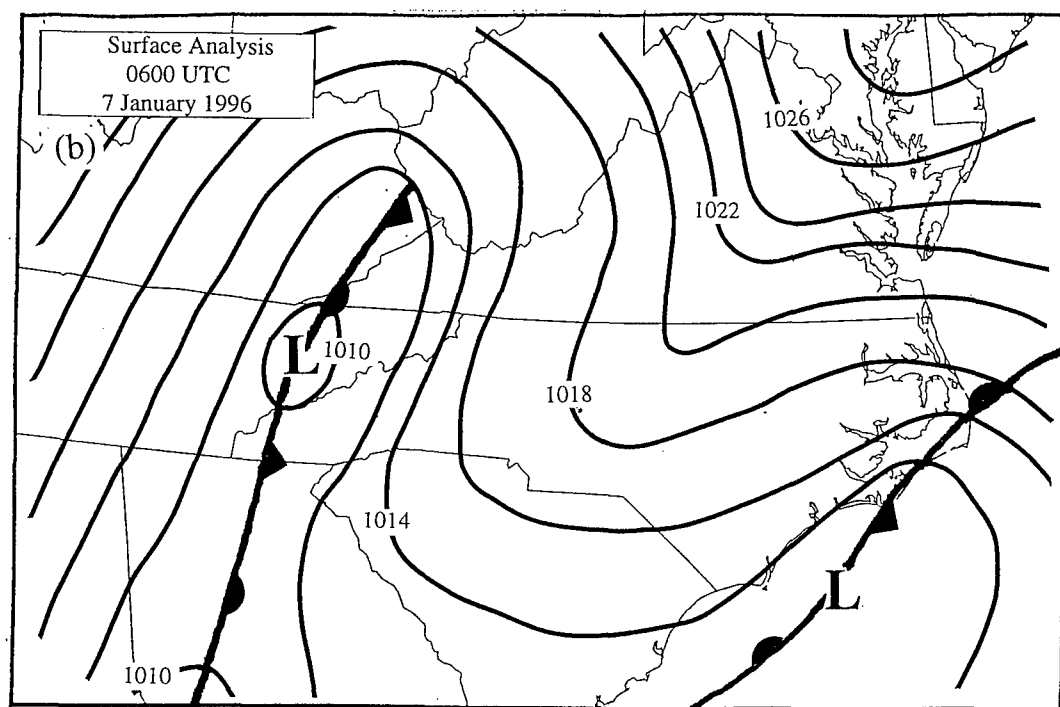
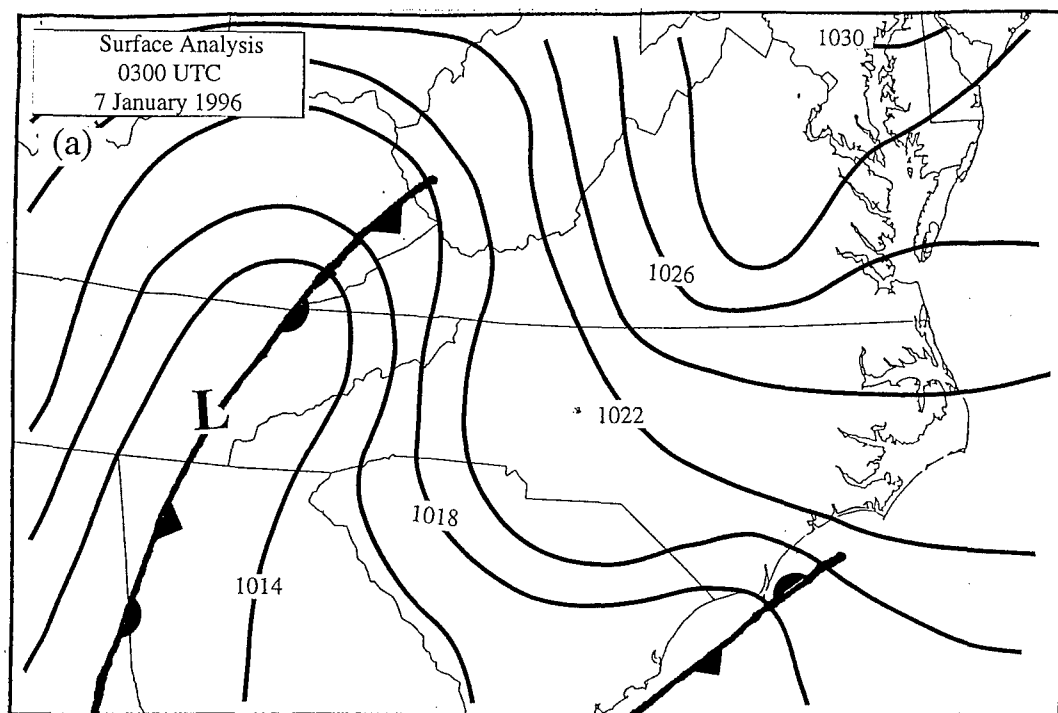


Figure 5.13. Same as Fig. 5.12 except for (a) 0300 UTC and (b) 0600 UTC.

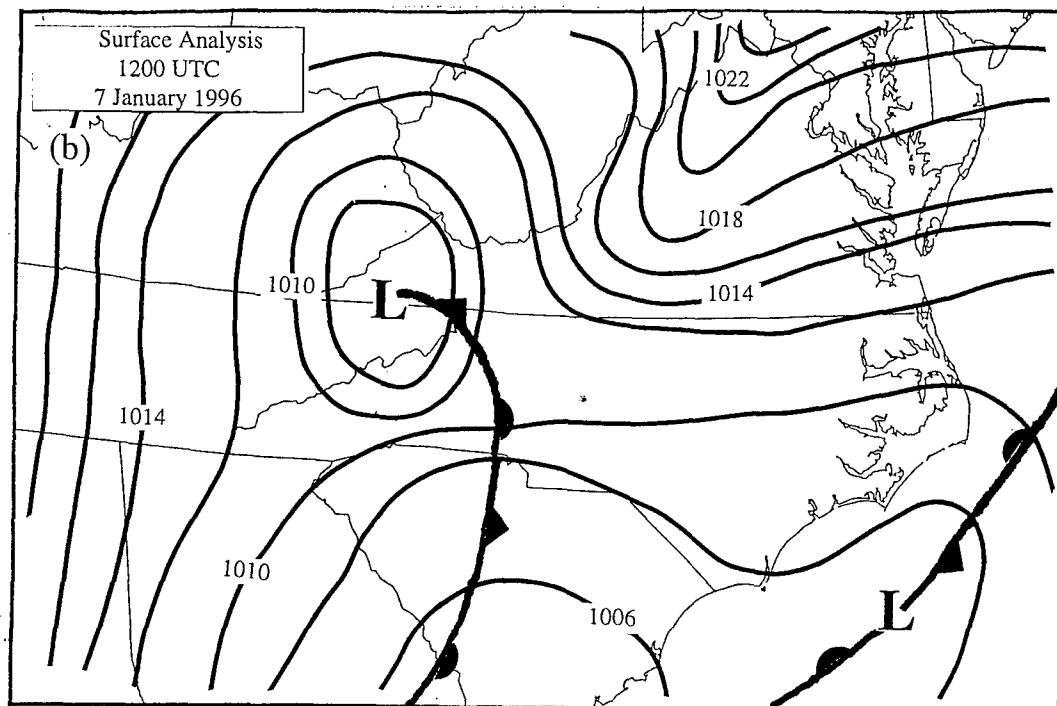
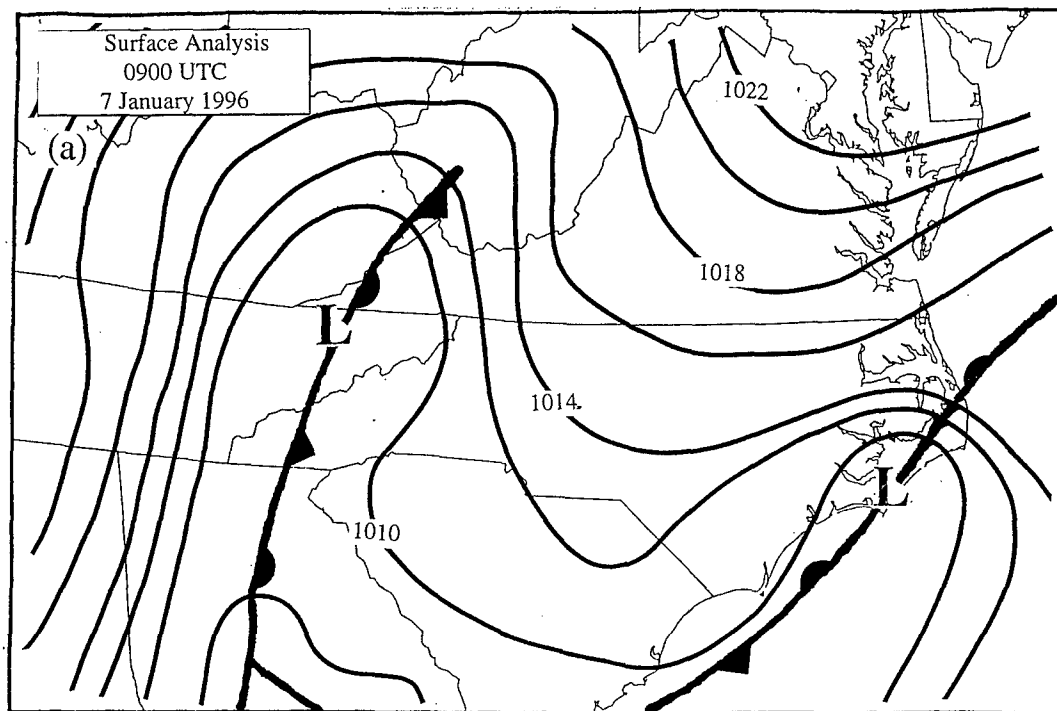


Figure 5.14. Same as Fig. 5.12 except for (a) 0900 UTC and (b) 1200 UTC.

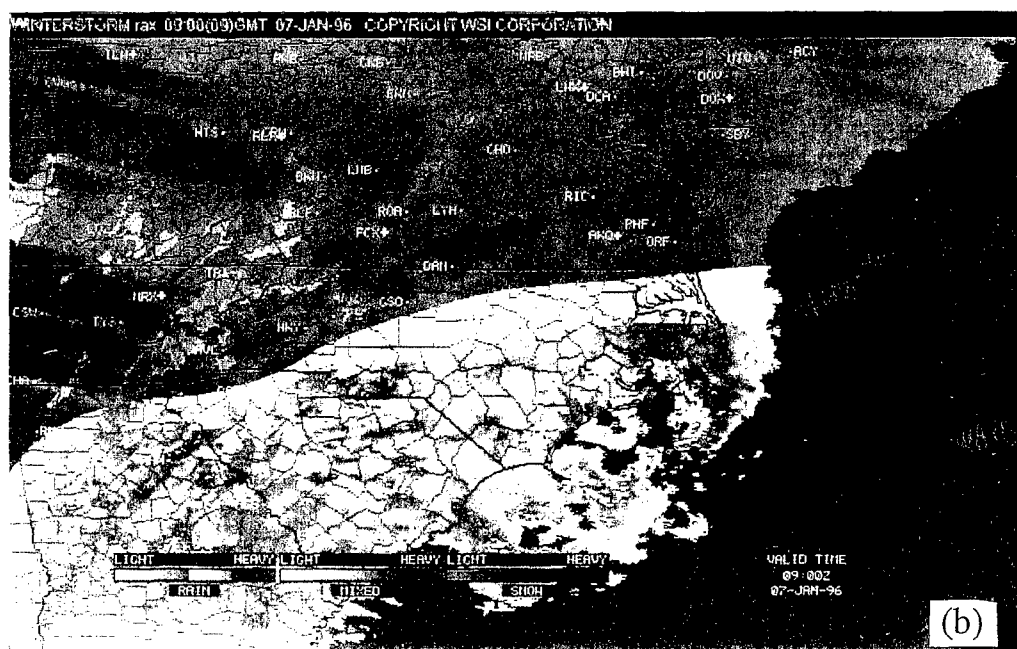
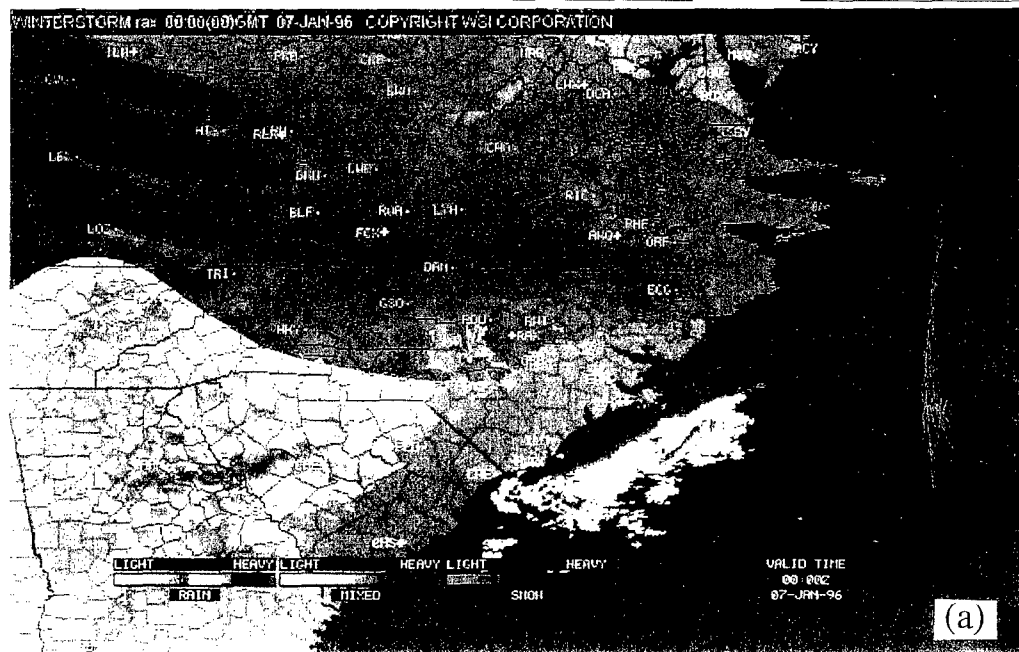


Figure 5.15 a) Regional radar composite for 7 January 1996 at 0000 UTC. Color codes are on bottom of figures. b) Regional radar composite for 7 January 1996 at 0900 UTC.

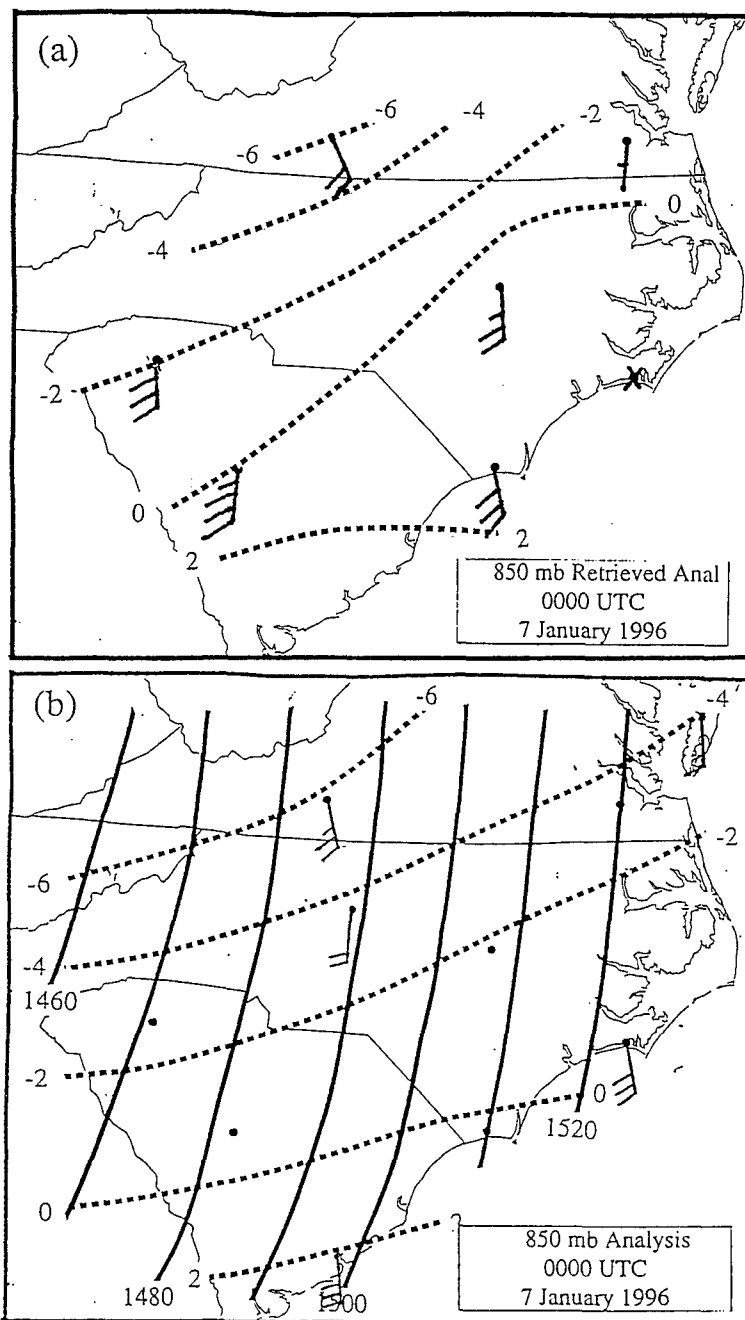


Figure 5.16. a) 850 mb analysis of retrieved temperature. Dotted lines are isotherms every 2°C for 0000 UTC 7 January 1996. b) 850 mb analysis for 0000 UTC 7 January 1996. Thin solid lines are height contours every 10 m and dotted lines are isotherms every 2°C. Winds represent VWP winds (kts) at 850 mb on (a).

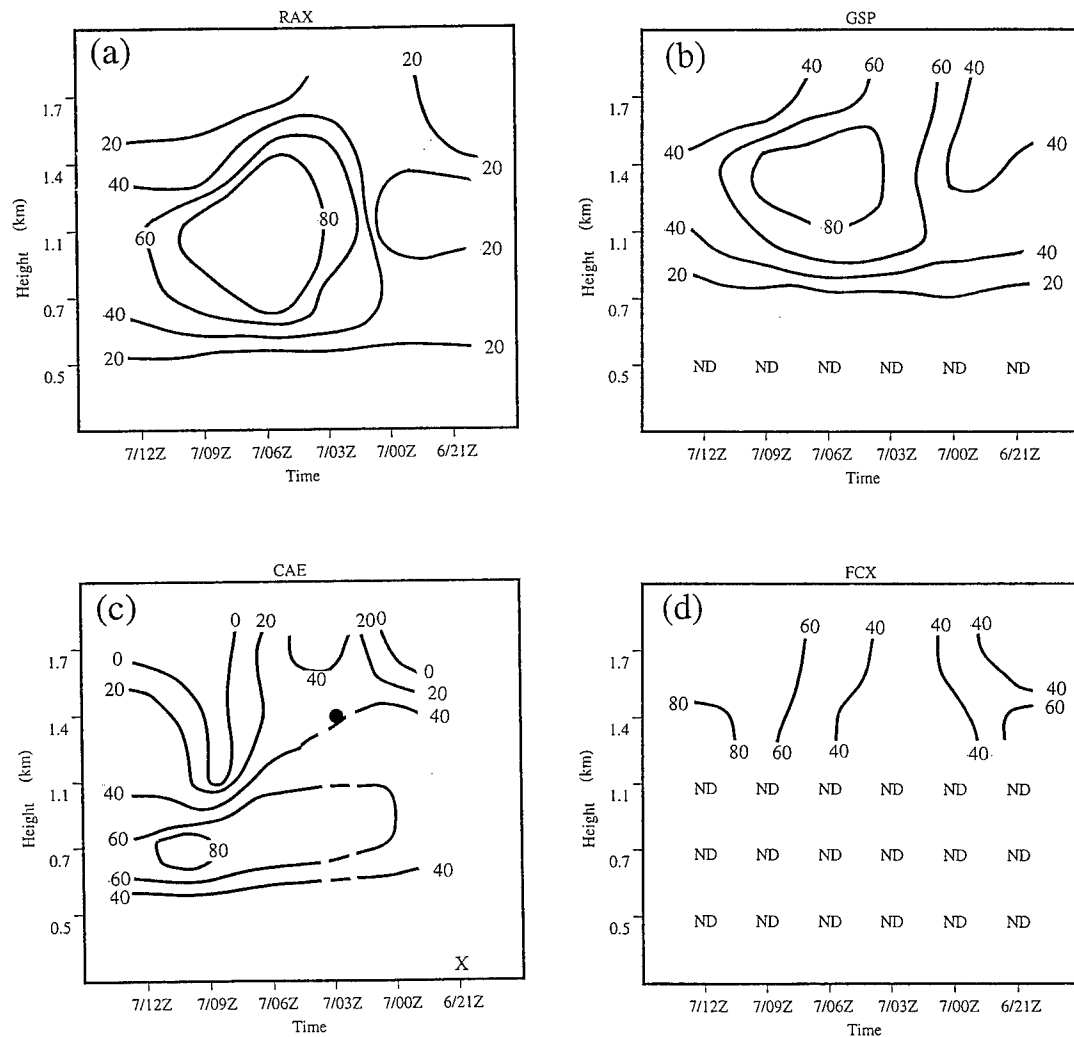


Figure 5.17. Temperature advection time-height cross sections for 6-7 January 1996. a) Raleigh, NC, b) Greenville/Spartanburg, SC, c) Columbia, SC, and d) Blacksburg, VA. Solid lines are temperature advection at intervals of 20°C/day (positive = warm advection). Dashed area indicates interpolation for a missing point. A dot indicates vertical interpolation of data point on VWPs. An X over a time period indicates all data missing for that time. ND means no data at that level (below ground). Heights on left are MSL.

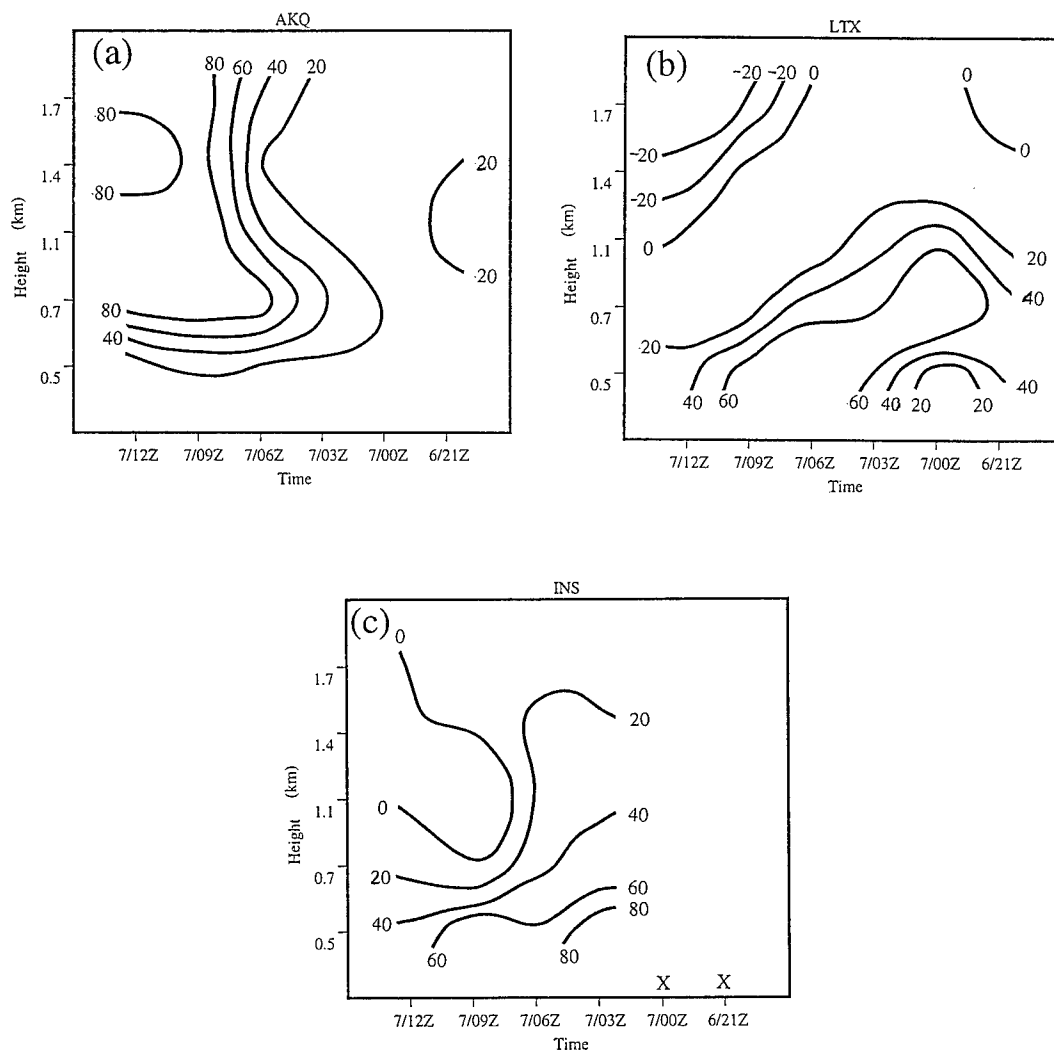


Figure 5.18 Same as Fig. 5.17 except for a) Wakefield, VA, b) Wilmington, NC, and c) Morehead City, NC.

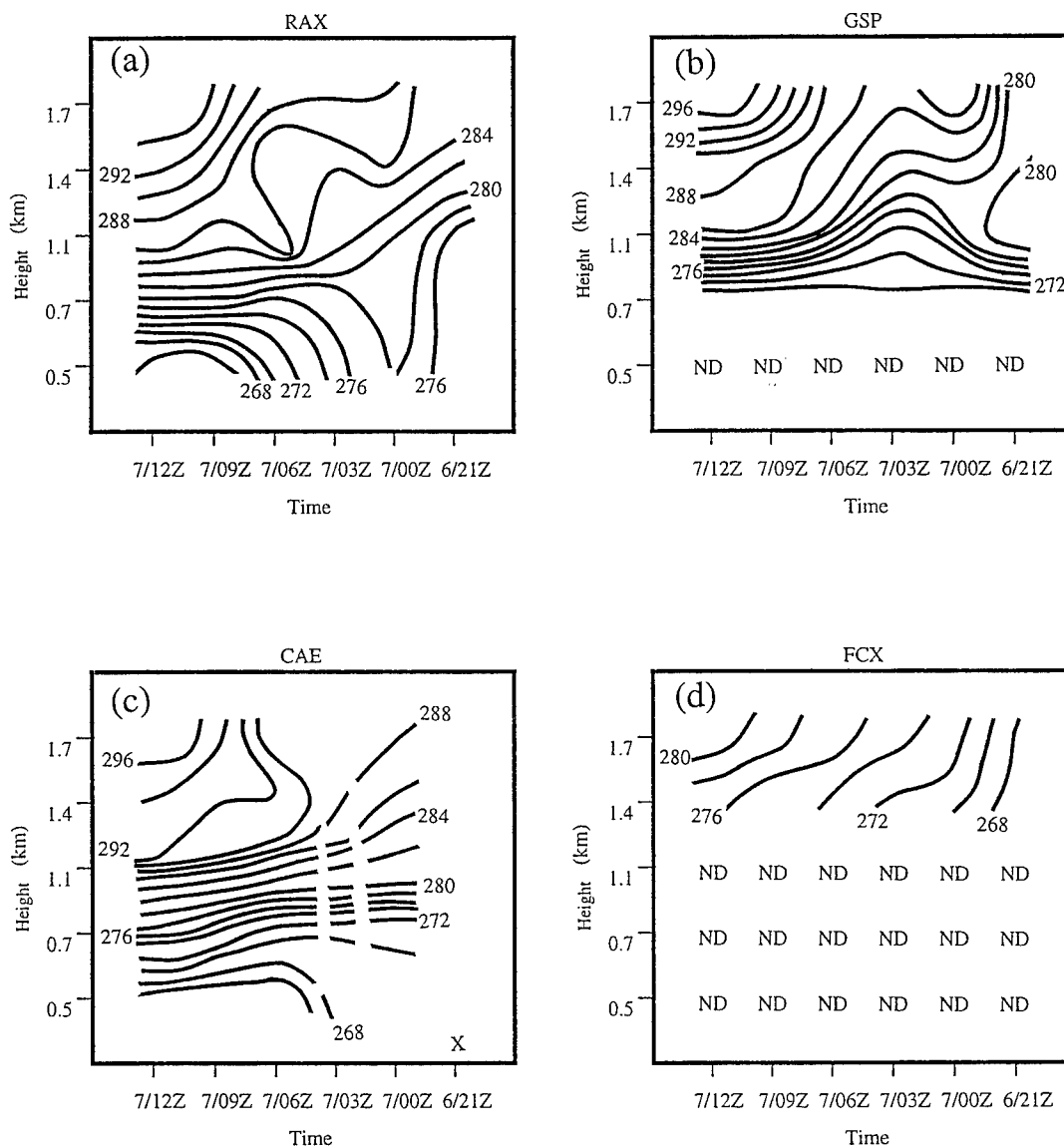


Figure 5.19. Isentropic time-height cross sections for 6-7 January 1996. a) Raleigh, NC, b) Greenville/Spartanburg, SC, c) Columbia, SC, and d) Blacksburg, VA. Solid lines are isentropes every 2°K. Dashed area indicates interpolation for a missing point. An X over a time period indicates all data missing for that time. ND means no data at that level (below ground). Heights on left are MSL.

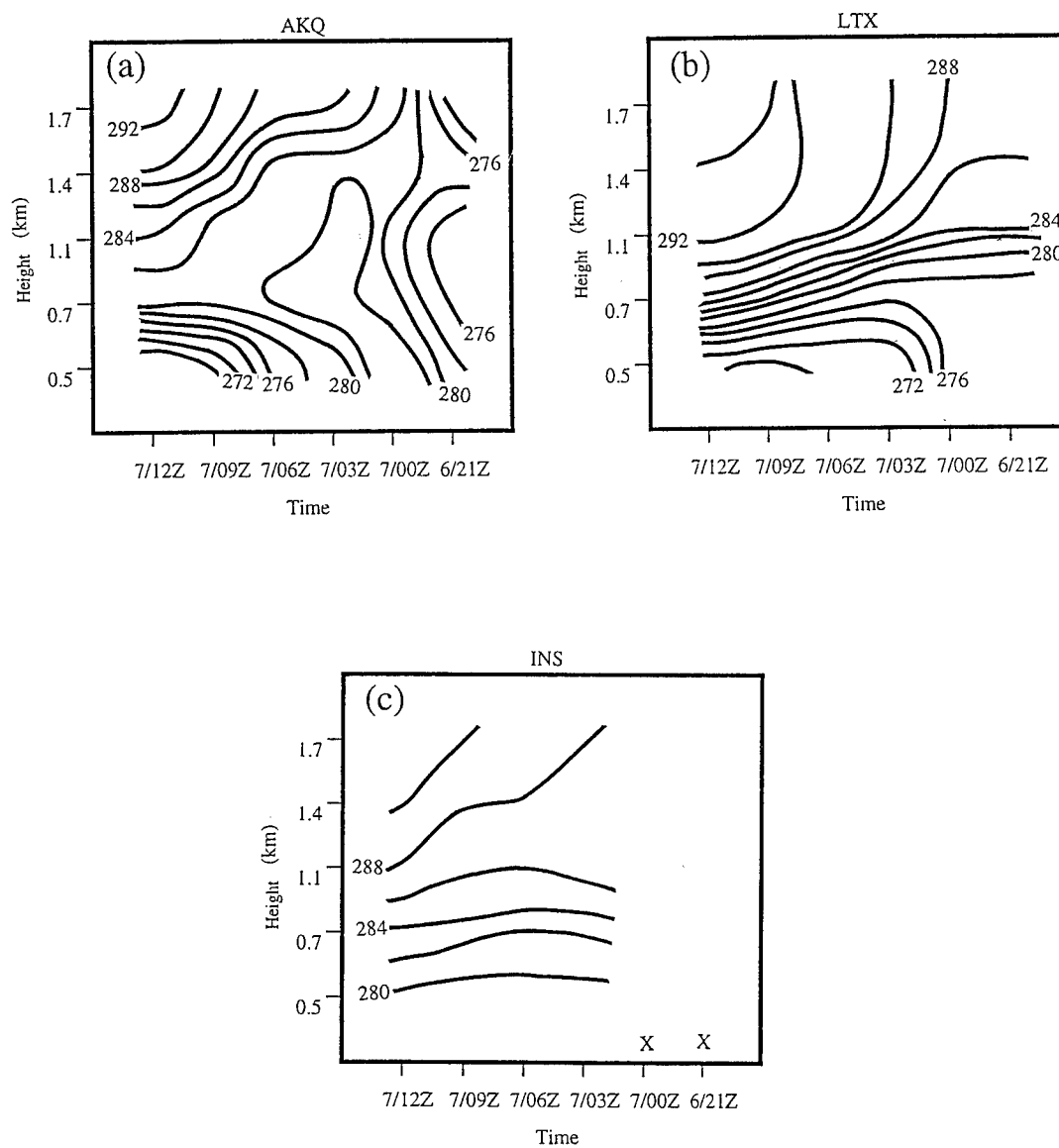


Figure 5.20. Same as Fig. 5.19 except for a) Wakefield, VA, b) Wilmington, NC, and c) Morehead City, NC.



## REFERENCES

- Ballentine, R. J., 1980: A numerical investigation of New England coastal frontogenesis. *Mon. Wea. Rev.*, **108**, 1479-1497.
- Bane, J. M. and D. A. Brooks, 1979: Gulf Stream meanders along the continental margin from the Florida Straits to Cape Hatteras. *Geophys. Res. Lett.*, **6**, 280-282.
- Bauman, W. H. III, 1989: Coastal frontogenesis and associated severe weather on 13 March 1986 (GALE IOP #13). M.S. thesis, Department of Marine, Earth and Atmospheric Sciences, North Carolina State University, 124 pp.
- Bell, G.D., and L. F. Bosart, 1988: Appalachian cold-air damming. *Mon. Wea. Rev.*, **116**, 137-161.
- Bosart, L. F., 1975: New England coastal frontogenesis. *Quart. J. Roy. Meteor. Soc.*, **101**, 957-978.
- , 1981: The Presidents' Day snowstorm of 18-19 February 1979: A subsynoptic-scale event. *Mon. Wea. Rev.*, **109**, 1542-1566.
- , and S. C. Lin, 1984: A diagnostic analysis of the Presidents' Day storm of February 1979. *Mon. Wea. Rev.*, **112**, 2148-2177.
- , and A. Seimon, 1988: A case study of an unusually intense atmospheric gravity wave. *Mon. Wea. Rev.*, **116**, 1857-1886.
- , C. J. Vaudo, and J. H. Helsdon Jr., 1972: Coastal frontogenesis. *J. Appl. Meteor.*, **11**, 1236-1258.
- Businger, S., W. H. Bauman III, and G. F. Watson, 1991: The development of the Piedmont front and associated severe weather on 13 March 1986. *Mon. Wea. Rev.*, **119**, 2224-2251.
- Chainé, P. M., 1973: Glaze and its misery: The ice storm of 22-23 March 1972 north of Montreal. *Weatherwise*, **26**, 124-127.
- Crum, T. D., and R. L. Alberty, 1993: The WSR-88D and the WSR-88D Operational Support Facility. *Bull. Amer. Meteor. Soc.*, **74**, 1669-1687.
- Crum, T. D., R. L. Alberty, and D. W. Burgess, 1993: Recording, archiving, and using WSR-88D data. *Bull. Amer. Meteor. Soc.*, **74**, 645-653.
- Dirks, R. A., J. P. Kuettner, and J. A. Moore, 1988: Genesis of Atlantic Lows Experiment (GALE): An overview. *Bull. Am. Meteorol. Soc.*, **69**, 148-160.
- Forbes, G. S., R. A. Anthes, and D. W. Thomson, 1987: Synoptic and mesoscale aspects of an Appalachian ice storm associated with cold-air damming. *Mon. Wea. Rev.*, **115**, 564-591.

- Forsythe, G. E., 1945: A generalization of the thermal wind equation to arbitrary horizontal flow. *Bull. Amer. Meteor. Soc.*, **26**, 371-375.
- Fritsch, J. M., J. Kopalka, and P. A. Hirschberg, 1992: The effects of subcloud-layer diabatic processes on cold air damming. *J. Atmos. Sci.*, **49**, 49-70.
- Haltiner, G. J., and R. T. Williams, 1980: *Numerical Prediction and Dynamic Meteorology*. John Wiley and Sons, 477 pp.
- Hartfield, G., Keeter, K.K., and Badgett, P., 1995: Cold air damming and damming look-alikes: a glossary of terms for field forecasters in the Carolinas and Virginia. (NWS internal memorandum).
- Holton, J.R., 1992: *An Introduction to Dynamic Meteorology*. Academic Press, 511 pp.
- Horton, C. W., 1984: Surface front displacement in the Gulf Stream by hurricane/tropical storm Dennis. *J. Geophys. Res.*, **89**, 2005-2012.
- Kaplan, M. L., J. W. Zack, V. C. Wong, and J. J. Tuccillo, 1982c: Initial results from a mesoscale atmospheric simulation system and comparisons with an AVE-SESAME I data set., *Mon. Wea. Rev.*, **110**, 1564-1590.
- Keeter, K. K., S. Businger, L. G. Lee, and J. S. Waldstreicher, 1995: Winter weather forecasting throughout the Eastern United States. Part III: The effects of topography and the variability of winter weather in the Carolinas and Virginia. *Wea. Forecasting*, **10**, 149-167.
- Klazura, G. E., and D. A. Imy, 1993: A description of the initial set of analysis products available from the NEXRAD WSR-88D system. *Bull. Amer. Meteor. Soc.*, **74**, 1293-1311.
- Knauss, J. A., 1978: *Introduction to Physical Oceanography*, Prentice-Hall, Inc., New Jersey, 338 pp.
- Koch, S.E., A. Aksakal, and J. T. McQueen, 1996: The influence of mesoscale humidity and evapotranspiration fields on a model forecast of a cold frontal squall line. *Mon Wea. Rev.* (in press).
- Kramer, D. P., S. E. Koch, and K. Waight, 1996: Mesoscale model analysis of a cold air damming event in the Carolinas during December 18-19, 1995. Preprints, *15th Conf. on Weather Analysis and Forecasting*, Norfolk, VA, Amer. Meteor. Soc.
- LaPenta, W. M., and N. Seaman, 1990: Numerical investigation of East Coast cyclogenesis during the cold air damming event of 27-28 February 1982. Part I: Dynamic and thermodynamic structure. *Mon. Wea. Rev.*, **118**, 2668-2695.
- Lee, R. R., J. L. Ingram, and G. E. Klazura 1994: A comparison of data from the WSR-88D VAD wind profile product and rawinsondes at twelve sites - preliminary results. Postprints, *1st WSR-88D Users' Conf.*, Norman, OK, WSR-88D Operational Support Facility.

- Manobianco, J., S. Koch, V. M. Karyampudi, and A. J. Negri, 1994: The impact of assimilating satellite-derived precipitation rates on numerical simulations of the ERICA IOP4 cyclone. *Mon. Wea. Rev.*, **122**, 341-365.
- , J. W. Zack, and G. E. Taylor, 1996: Workstation-based real-time mesoscale modeling designed for weather support to operations at the Kennedy Space Center and Cape Canaveral Air Station. *Bull. Amer. Meteor. Soc.*, **77**, 653-672.
- Marks, F. D., and J. M. Austin, 1979: Effects of the New England coastal front on the distribution of precipitation. *Mon. Wea. Rev.*, **107**, 53-67.
- MASS, 1994: MASS version 5.6 Reference Manual, MESO Inc., 185 Jordan Rd. Troy, NY 12180.
- Miller, J. E., 1946: Cyclogenesis in the Atlantic coastal region of the United States. *J. Meteorol.*, **3**, 31-44.
- Neiman, P. J., P. T. May, and M. A. Shapiro, 1992: Radio acoustic sounding system (RASS) and wind profiler observations of lower- and midtropospheric weather systems. *Mon. Wea. Rev.*, **120**, 2298-2313.
- , P. T. May, B. B. Stankov, and M. A. Shapiro, 1991: Radio acoustic sounding system observations of an arctic front. *J. Appl. Meteor.*, **30**, 881-892.
- , and M. A. Shapiro, 1989: Retrieving horizontal temperature gradients and advections from single-station wind profiler observations. *Wea. Forecasting*, **2**, 222-233.
- Nielsen, J. W., 1989: The formation of New England coastal fronts. *Mon. Wea. Rev.*, **117**, 1380-1401.
- Penn, S., 1957: The prediction of snow vs rain. Forecasting Guide No. 2, U.S. Weather Bureau, 299 pp.
- Richwein, B. A., 1980: The damming effect of the southern Appalachians. *Natl. Wea. Dig.*, **5**, 2-12.
- Riordan, A. J., 1990: Examination of the mesoscale features of the GALE coastal front of 24-25 January 1986. *Mon. Wea. Rev.*, **118**, 258-282.
- , 1996: The coastal front: An historical perspective. Preprints, *Conf. on Coastal Oceanic and Atmospheric Prediction*, Atlanta, GA, Amer. Meteor. Soc.
- , J. Thomas Anderson, and S. Chiswell, 1995: Small-scale structure of a coastal front as revealed by Dual-Doppler Radar. *Mon. Wea. Rev.*, **123**, 622-640.
- , S. Raman, J. M. Davis, and S. Viessman, 1985: Measurements in the marine boundary layer near a coastal front. *Geophys. Res. Lett.*, **12**, 681-684.

- Souza, C. A., 1994: The operational forecasting/nowcasting of precipitation type in the southeastern United States. Type of precipitation: Descriptive and objective guidance. M.S. thesis. Department of Marine, Earth and Atmospheric Sciences, North Carolina State University, 116 pp.
- Stull, R.B., 1994: *An Introduction to Boundary Layer Meteorology*. Kluwer Academic Publishers, 666 pp.
- Vescio, M. D., K. K. Keeter, G. Dial, P. Badgett, and A. J. Riordan, 1993: A low-top weak-reflectivity severe weather episode along a thermal/moisture boundary in eastern North Carolina. Preprints, *17th Conf. on Severe Local Storms*, St. Louis, MO, Amer. Meteor. Soc., 629-633.